An integrated modeling study on the effects of mineral dust and sea salt particles on clouds and precipitation.

S. Solomos[1], G. Kallos[1], J. Kushta[1], M. Astitha[1,2],C. Tremback[3], A. Nenes[4,5] and Z. Levin[6]

[1] University of Athens, School of Physics, University of Athens Campus, Bldg. Phys-5, 15784 Athens, Greece

[2]Energy, Environment and Water Research Centre, The Cyprus Institute, Nicosia, Cyprus

[3]ATMET LLC P.O. Box 19195, Boulder, CO 80308-2195, USA

[4]School of Chemical and Biomolecular Engineering, Georgia Institute of Technology, USA

[5]School of Earth and Atmospheric Sciences, Georgia Institute of Technology, USA

[6]Dept. of Geophysics and Planetary Sciences, Tel Aviv University, Tel Aviv, Israel

Corresponding Author: kallos@mg.uoa.gr

July 2010

Abstract

The amount of airborne particles that will nucleate and form cloud droplets under specific atmospheric conditions, depends on their number concentration, size distribution and chemical composition. Aerosol is affected by primary particle emissions, gas-phase precursors, their transformation and interaction with atmospheric constituents, clouds and dynamics. A comprehensive assessment of these interactions requires an integrated approach; most studies however decouple aerosol processes from cloud and atmospheric dynamics and cannot account for all the feedbacks involved in aerosol-cloud-climate interactions. This study addresses aerosol-cloud-climate interactions with the Integrated Community Limited Area Modeling System (ICLAMS) that includes online parameterization of the physical and chemical processes between air quality and meteorology. ICLAMS is an extended version of the Regional Atmospheric Modeling System (RAMS) and it has been designed for coupled air quality – meteorology studies. Model sensitivity tests for a single-cloud study as well as for a case study over the Eastern Mediterranean illustrate the importance of aerosol properties in cloud formation and precipitation. Mineral dust particles are often coated with soluble material such as sea-salt, thus exhibiting increased CCN efficiency. Increasing the percentage of salt-coated dust particles by 15% in the model resulted in more vigorous convection and more intense updrafts. The clouds that were formed extended about three kilometres higher and the initiation of precipitation was delayed by one hour. Including on-line parameterization of the aerosol effects improved the model bias for the twenty-four hour accumulated precipitation by 7%. However, the spatial distribution and the amounts of precipitation varied greatly between the different aerosol scenarios. These results indicate the large portion of uncertainty that remains unresolved and the need for more accurate description of aerosol feedbacks in atmospheric models and climate change predictions.

1. *Introduction*

Aerosols are a mixture of natural and anthropogenic particles. Mineral dust, sea-salt, primary biogenic particles and volcanic ash originate from natural sources, while anthropogenic particles originate from industrial activity, fossil-fuel and biomass burning. Aerosol particles directly affect the radiation budget of the atmosphere by absorbing and/or scattering radiation across the solar and long-wave radiation spectrum (Charlson et al., 1992; IPCC, 2001; Myhre et al., 2003b; Seinfeld et al., 2004; Ramanathan et al. 2007). Additionally, they influence the nutrient dynamics and biogeochemical cycling of both terrestrial and oceanic ecosystems and may have considerable impacts on human health (Dockery and Pope, 1994; Herut et al., 2002; Meskhidze et al., 2003,2005; Meskhidze and Nenes 2006; Mahowald et al., 2008; Mitsakou et al., 2008). Airborne particles serve as cloud condensation nuclei (CCN) and ice nuclei (IN); changes thereof can affect the cloud cover, radiative properties, the distribution of precipitation and the hydrological cycle in general (Twomey et al., 1977; Albrecht 1989; De Mott et al., 2003; Sassen et al., 2003; Andreae and Rosenfeld, 2008). Quantifying the number of particles that act as CCN , as well as the number of particles that can initiate heterogeneous ice formation processes (ice nuclei, IN) is essential for determining the role of aerosols in cloud and precipitation processes (e.g., Lohmann and Feichter, 2005; Levin and Cotton, 2009). Moreover, formation of secondary particles and atmospheric ageing of aerosol lead to particles with substantially different properties than those at source regions (Seinfeld and Pandis 1998; Levin et al., 1996; Wurzler at al., 2000; Jacobson 2001; Chung and Seinfeld 2002).

Mineral dust and sea salt are major components of particulate matter in the atmosphere. Desert dust accounts for more than 50% of the global aerosol load (Andreae et al. 1986; Zender et al., 2005) and the long range transport of dust particles can influence the composition and dynamic state of the atmosphere thousands of kilometers downwind of their source region (Kallos et al., 2007). Under favourable conditions, dust particles originating from Northern and Central Africa may get elevated and travel towards Atlantic and Caribbean (Karyampudi, 1979; Karyampudi et al., 1999; Prospero et al., 2005; Kallos et al., 2006) or cross the Mediterranean towards Europe affecting both air quality and meteorology in Southern Europe (Mitsakou et al., 2008 ; Querol et al., 2009). Dust particles are efficient ice nuclei (IN) and contribute to the formation of ice particles in high clouds (DeMott et al., 2003a; Teller and Levin 2006). Also they interact with sea salt or anthropogenic pollutants, mainly sulfates and nitrates, thus forming particles that consist of a core of

mineral dust with coatings of soluble material (Levin et al., 2006). The soluble coating on the dust particles converts them into efficient CCN while maintaining their ability as IN (Levin et al., 2006; Astitha and Kallos, 2008 ; Astitha et al., 2010). Sea-salt particles are also very efficient CCN and is the dominant source of particulate matter in the marine boundary layer (Gong at al., 2002 ; Pierce and Adams, 2006). The amount of particles that can act as CCN and activate to cloud droplets depends on the concentration of available particles, their size distribution and their chemical composition (e.g., Köhler, 1936; Charlson et al., 2001; Nenes et al., 2002). Additionally, absorption of solar radiation by dust, results in heating of the dust layer and subsequently in modification of the thermodynamic structure of the atmosphere, thus leading to suppression or enhancement of precipitation depending on the type of the clouds (Yin and Chen, 2007). The interplay between cloud dynamics and the composition of the atmosphere may delay the initiation of precipitation or steer a storm towards a different location and precipitation amounts will vary accordingly (Lynn et al., 2005b ; van den Heever and Cotton, 2007 ; Rosenfeld at al., 2007 ; Zhang et al., 2007 ; Cotton et al., 2007).
By modifying the microphysical, optical and radiative properties of clouds, dust and salt particles contribute to the indirect aerosol effect and introduce significant uncertainty in assessments of anthropogenic climate change (Charlson et al., 1990; Lohmann and Feichter, 2005; IPCC, 2007; Andreae and Rosenfeld, 2008). The effects of dust and sea salt on regional climate depend also on the local topography and soil characteristics (e.g., Junkermann et al., 2009) and cloud type (Seifert and Beheng, 2006). Therefore, the effects of atmospheric composition on clouds and precipitation are not monotonic and may differ from one area to another.

The complexity of the above processes and the possible interactions and feedbacks across all scales in the climate system, indicate the need for an integrated approach in order to examine the impacts of air quality on meteorology and vice versa (Stevens and Feingold, 2009). This study adopts such an approach to study an idealized case representative of mid-latitude marine boundary layers and a specific test case over eastern Mediterranean. A description of the new model developments is described in Section 2. Section 3 includes idealized sensitivity tests as well as the analysis of an experimental case. Finally the main results are summarized in Section 4.

2. Description of ICLAMS

The Regional Atmospheric Modeling System (RAMSv6) (Pielke et al., 1992; Cotton et al. 2003) was the basis for developing the Integrated Community Limited Area Modeling System (ICLAMS) used in this study. This new version of the model has been designed for air pollution and climate research applications and includes several new capabilities related to physical and chemical processes in the atmosphere. The model components are summarised in Table 1; new developments include an interactive desert-dust and sea-salt cycle, biogenic and anthropogenic pollutants cycle, gas/cloud/aerosol chemistry, explicit cloud droplet nucleation scheme and an improved radiative transfer scheme. Each process is in modular form, and each component can be activated / deactivated during a simulation. The two-way interactive nesting capabilities of the model allow the use of regional scale domains together with several high resolution nested domains. This feature is important for the purpose of the present work since it allows for simultaneous description of long range transport phenomena and aerosol-cloud interactions at cloud resolving scales. The explicit two-moment cloud microphysics scheme of the model is used to describe the aerosol-cloud interactions. The dust and sea salt cycles parameterization together with the radiative transfer and cloud droplet nucleation modules of the model are described in the following sections.

2.1 Mineral Dust

The dust-cycle simulation adopts the approach of the SKIRON/Dust model (Spyrou et al., 2010) and is based on the "saltation and bombardment" mechanism (Marticorena and Bergametti, 1995 ; Lu and Shao, 1999 ; Alfaro and Gomez, 2001; Grini et al., 2002). The model contains 22 land-use categories (Table 2). All grid cells classified as "desert" or "semi-desert" are treated as potential dust sources. Saltation occurs when the friction velocity exceeds a characteristic threshold, u_f. For the mobilization of sand particles, u_f is calculated based on the friction Reynolds number (Marticorena et al., 1997b; Zender at al., 2003) and the soil wetness for each particular model grid point (Fécan et al., 1999). Upon mobilization, sand grains (>60 μm) are elevated a few meters above ground; upon resettling, the grains "bombard" the soil and eject secondary silt (2.5-60 μm) and clay (<2.5 μm) particles. These particles are sufficiently small to remain suspended, get transferred by turbulence within the ABL and then to free troposphere from where they can be transported thousands of kilometers away from their source. The efficiency with which the mineral dust particles are transported vertically is strongly sensitive to their size distribution. The finest particles are small enough to be transported to long distances while larger particles can only be transported to distances near their sources. Based on this approach, the vertical dust flux is distributed into three lognormal source modes with different shapes and mass fractions. The transport mode is represented inside the model with eight discrete size bins as in Perez et al., (2006a) and Spyrou et al., (2010) with effective radii of 0.15, 0.25, 0.45, 0.78, 1.3, 2.2, 3.8, and 7.1 μm respectively. Each dust bin is treated as a scalar variable for advection and diffusion purposes. Partitioning of the dust spectrum and separate treatment of each size mode is important for the description of size dependent processes such as dry and wet deposition, CCN activation and radiative transfer.

2.2 Sea salt spray

The sea salt aerosol emission fluxes depend strongly on the meteorological conditions close to the air-sea surface. The most prominent mechanism for the generation of sea salt aerosols is the bursting of entrained air bubbles during whitecap formation due to surface wind. The method follows the open sea white - cap formation as described in Monahan et al., (1986) which gives a continuous particle-size distribution at a specific relative humidity (RH), usually 80%.

$$\frac{dF_{N-Open}}{dr_{80}} = 1.373 \cdot \mathrm{u}_{10}^{3.41} \cdot r_{80}^{-A} \cdot \left(1 + 0.057 r_{80}^{3.45}\right) \cdot 10^{1.607 e^{-B^2}} \qquad (1)$$

$$A = 4.7 \cdot \left(1 + \Theta r_{80}\right)^{-0.017 r_{80}^{-1.44}}, \Theta = 30 \qquad (2)$$

$$B = \left(0.433 - \log r_{80}\right)/0.433 \qquad (3)$$

where u_{10} is the wind speed at 10m height, and r_{80} is the particle radius at 80% RH. This semi-empirical formulation is based on laboratory measurements for particles with radius 0.8–8 μm. The size range of the sea-salt source function has been extended to below 0.1 μm in radius based on the parameterization proposed by Gong, (2003). Additionally, in order to take into account the hygroscopic nature of sea salt, the size distribution of the particles is calculated as a function of local RH following Zhang et al., (2005). This method accounts for the hygroscopic uptake of water from sea salt particles for RH values between 45% and 99%.

Whitecaps may also occur along coastal zones at lower wind speeds than in open seas because of breaking of internal waves when they interact with the sea bottom and shore. The sea salt aerosols produced over the surf zone provide an additional surface for heterogeneous reactions and have a significant impact on PM concentrations in marine areas (Seinfeld and Pandis, 1998). Coastline sea salt flux is also parameterized in the model following the work of Leeuw et al., (2000) and Gong et al., (2002).

Sea salt particle spectrum is represented with a bimodal lognormal distribution assuming a mean diameter of 0.36 μm for the first (accumulated) mode and a mean diameter of 2.85 μm for the second (coarse) mode. Geometric dispersion is 1.80 and 1.90 for the two modes respectively.

2.3 Dry deposition

Dry deposition for dust and salt particles is treated as a first order removal process, equal to the concentration multiplied by a mass transfer coefficient, V_d (termed “deposition velocity”; Seinfeld and Pandis, 1998; Slinn and Slinn, 1980). V_d accounts for the effects of reactivity, hygroscopic water uptake, size distribution of particles, meteorological conditions and surface characteristics. Wesely (1989) proposed a resistance model to account for all the elements described above; dry deposition fluxes are controlled by gravitational settling, turbulent mixing, and Brownian diffusion across two virtual layers. In the layer adjacent to the surface, Brownian diffusion (for small particles) and gravitational settling (for large particles) are the main deposition processes. In the second layer, called the “constant flux layer”, turbulent mixing and gravitational settling dominate deposition. V_d of a particle with a given diameter is then parameterized using a set of mass transfer resistances associated with the combined effects of these processes in both layers (Wesely, 1989; Seinfeld and Pandis, 1998) :

$$r_a = \frac{1}{ku_*}\left[\ln\left(\frac{1}{z_0}\right) - \phi_h\right] \quad (4)$$

$$r_b = \frac{1}{u_*\left(\mathrm{S_c}^{-2/3} + 10^{-3/\mathrm{S_t}}\right)} \quad (5)$$

$$V_d = V_{sed} + \frac{1}{r_a + r_b + r_a r_b V_{sed}} \quad (6)$$

where r_a is the aerodynamic resistance, r_b is the boundary resistance, k is the von Karman constant, z_o is the surface roughness length, φ_h a stability correction term, $\mathrm{S_c}$ is the Schmidt number, $\mathrm{S_t}$ is the Stokes number and V_{sed} is the gravitational settling velocity.

2.4 Wet deposition

Proper treatment of the wet removal process is essential for a realistic aerosol simulation, since it is the predominant removal process for atmospheric particles away from their sources. The amount of particles removed at each model timestep from in-cloud and below-cloud scavenging is expressed as:

$$\frac{\partial C}{\partial t} = -\Lambda C \quad (7)$$

where Λ is the "scavenging coefficient" of the aerosols. For in-cloud removal, Λ is calculated from the droplet-aerosol collection efficiency (E), the precipitation rate (P) and the radius of the scavenging droplet (r_d) following the formulation of Seinfeld and Pandis (1998):

$$\Lambda = \frac{3}{4}\frac{EP}{r_d} \quad (8)$$

The collection efficiency (E) for a particle of radius (r_p) is calculated from the contribution of Brownian diffusion, turbulent diffusion, interception, inertial impaction and electric forces (Slinn, 1984; Seinfeld and Pandis, 1998):

$$E(r_p) = \frac{4}{\mathrm{Re}\,\mathrm{S_c}}\left(1 + 0.4\,\mathrm{Re}^{1/2}\,\mathrm{S_c}^{1/3} + 0.16\,\mathrm{Re}^{1/2}\,\mathrm{S_c}^{1/2}\right) +$$

$$+ 4\phi\left[\frac{\mu}{\mu_w} + \phi\left(1 + \mathrm{Re}^{1/2}\right)\right] + \left[\frac{\mathrm{S_t} - \mathrm{S}^*}{\mathrm{S_t} - \mathrm{S}^* + 2/3}\right]^{3/2} \qquad (9)$$

where Re is the droplet Reynolds number, $\mathrm{S_c}$ is the particle Schmidt number, r_d is the droplet radius, $\phi = \frac{r_p}{r_d}$, μ, μ_w are the kinematic viscosities of the air and liquid water, respectively, $\mathrm{S_t}$ is the particle Stokes number and

$$S^* = \frac{1.2 + \ln(1 + \mathrm{Re})/12}{1 + \ln(1 + \mathrm{Re})} \qquad (10)$$

2.5 ICLAMS Radiation scheme

The basic options for shortwave/longwave radiative transfer in RAMS include the Chen and Cotton (1983) and the Harrington (1997) schemes. The former treats all hydrometeors as liquid-phase; the latter scheme includes three shortwave and five infrared bands interacting with ice and liquid condensates and with model gases. Radiation transfer calculations options in ICLAMS have been extended with the implementation of the Rapid Radiative Transfer Model (RRTM) for both SW and LW bands (Mlawer et al., 1997; Iacono et al., 2000). RRTM is a spectral-band radiative transfer scheme based on the correlated-*k* method (Lacis and Oinas, 1991; Fu and Liou, 1992). Pre-calculated look-up tables are used to simulate the impact of clouds and the impact of various atmospheric gases and aerosols in the distribution of the radiation along the atmosphere. For both Harrington and RRTM radiation options, the aerosol optical depth of prognostic dust has been also added to the calculation of the total optical depth to account for its direct radiative forcing and photochemical impacts.

2.6 Cloud droplet nucleation parameterization

RAMS has been widely used for cloud research during the last two decades (Krichak and Levin, 2000 ; Mavromatidis and Kallos, 2003 ; Saleeby and Cotton, 2004 ; Van den Heever et al., 2006 ; Van den Heever and Cotton, 2007 ; Mavromatidis et al., 2007 ; Zhang et al., 2007 among others). The model is able to explicitly resolve a complete set of atmospheric processes at resolutions ranging from tens of kilometers down to a few meters. The nesting capabilities of the model allow for sufficient representation of microphysical processes at cloud scales. RAMS includes eight categories of hydrometeors (vapor, cloud droplets, rain droplets, pristine ice, snow, aggregates, graupel and hail). The two-moment microphysics parameterization scheme treats both the mixing ratio and number concentration of each hydrometeor (Meyers et al., 1997). Prediction of cloud droplet number concentration is originally based on air temperature, vertical wind component and on a constant amount of available CCN. A lookup table has been constructed offline from a detailed bin-parcel model and the number of activated CCN is calculated from this table. The size and chemical properties of the CCN are not taken into consideration. This approach has been altered in the new version of the model with the addition of an explicit cloud droplet nucleation parameterization scheme (Nenes and Seinfeld, 2003; Fountoukis and Nenes, 2005). This scheme (referred to as FNS), provides a comprehensive microphysical link between aerosols and clouds. FNS computes droplet number based on the parcel framework, and solves for the maximum supersaturation, s_{max}, that develops given a set of cloud-scale dynamics (temperature, pressure and vertical wind component) and aerosol properties (number concentration, size distribution and chemical composition). The droplet number is then equal to the number of CCN with critical supersaturation less or equal to s_{max} (Nenes and Seinfeld, 2003). The water vapour uptake coefficient, used in calculating the mass transfer coefficient of water vapour to growing droplets (Fountoukis and Nenes, 2005), is set to 0.06 based on in-situ cloud droplet closure experiments (Meskhidze et al., 2005; Fountoukis et al., 2007).

Soil dust, sea salt spray and secondary pollutants contribute to the CCN population. Dust particles are assumed to follow a lognormal size distribution at source regions. The properties of these distributions (number mean diameter and geometric dispersion) are expected to change throughout their atmospheric lifetime. These properties are explicitly calculated at every model step based on the predicted dust concentration (Shultz et al., 1998). CCN concentrations are expressed as a function of supersaturation using Köhler theory (Köhler, 1936; Nenes and Seinfeld, 2003).

Freshly-emitted mineral dust particles have long been known to act as effective ice nuclei (Pruppacher and Klett 1997; DeMott et al., 2003, Levin et al., 2005). Ice production is generally facilitated over regions with high mineral dust concentrations, such as over the Atlantic Ocean during African dust transportation episodes (Astitha et al., 2010). In ICLAMS, the insoluble fraction of dust contributes to the prognostic ice-forming nuclei (IFN) following the formulation of Meyers et al., (1992).

3 Clouds and precipitation in an environment with natural particles

3.1 Idealized simulations

In order to examine the sensitivity of the new cloud nucleation scheme to aerosol properties, we performed a set of "idealized" simulations for a convective cloud system over flat terrain. The model was configured on a two-dimensional domain with horizontal uniform resolution of 300m and 35 vertical levels, starting from 50m spacing near the ground and extending up to 18km with a geometric stretching ratio of 1.2. The horizontal dimension of the domain was 24km. The model was initialized from a convectively unstable sounding (Figure1) that is considered as representative of winter weather type for the eastern Mediterranean region (Yin et al., 2002; Levin et al., 2005). Initial wind conditions of 3 m s^{-1} wind speed and a western wind direction were applied homogeneously over the domain. The FNS parameterization was invoked in every time step and grid point and the number of activated droplets was calculated from grid-cell aerosol, P, T, and updraft velocity. All tests were performed with exactly the same configuration except for the aerosol properties. Each run started at 12:00 UTC and lasted for six hours.

Two scenarios were considered for the initial distribution of aerosol concentration, namely the "pristine" and the "hazy" scenario as illustrated in Figure 2. The "pristine" scenario is representative of a remote area with a relatively clean atmosphere of total particle concentration 100 cm^{-3}, while the "hazy" scenario assumes a total concentration of 1500 cm^{-3} similar to Teller and Levin (2006). Such high aerosol concentrations can be found near urban areas or industrial zones and are also typical during intense dust episodes. The size distribution of the particles was considered to follow a bimodal lognormal distribution that does not change shape between scenarios. The geometric standard deviation equals two for both modes, while the number median diameter was set at 0.2 μm for the first mode and at 2 μm for the second mode. The chemical composition for the soluble fraction of the particles was assumed to be ammonium sulfate and the aerosol field was applied homogeneously throughout the model domain. Further development of the cloud system and the final amount of precipitation depend on the cloud microphysical structure and on the interplay with ambient dynamics. Both runs started developing a similar cloud structure after 80 minutes of simulation time and, as seen in Figure 3, two distinctive convective areas were identified within a horizontal distance of about 15 km. However, after the initial development, the cloud properties varied significantly between the "pristine" and "hazy" scenarios. These changes are reflected in the hourly accumulated precipitation over the entire domain and in the maximum values of mixing ratios and number concentrations for cloud droplets, rain droplets and pristine ice particles that are summarized in Table 3 for each model run.

In the "pristine" simulation, the cloud droplets number concentration remained low (maximum of 130 cm^{-3}) throughout the simulation. Fewer CCN had to compete for the same amount of water. So, large cloud and rain droplets were allowed to develop and the collection efficiency was enhanced. This allowed for increased autoconversion rates of cloud to rain droplets and early initiation of warm rain process. Intense precipitation started 100 minutes into the simulation, with precipitation rates reaching as high as 15 mm h^{-1} (Figure 4). The high rain mixing ratio peak value (0.47 g kg^{-1}) and corresponding rain drop number concentration of 27.65 l^{-1} indicate the dominance of collision-coalescence during the early stages of the cloud.

In contrary, the "hazy" clouds suppressed precipitation at the early cloud stages. The number of cloud droplets was extremely high, especially during the first two hours of cloud development and reached 2133 cm^{-3} after 120 minutes of run. As a result, the conversion rates of cloud droplets to rain droplets were very low and precipitation was inhibited. Maximum precipitation rate at this stage was only 4 mm h^{-1} which is about 4 times less than the "pristine" scenario. However, pristine ice particles were almost double that of the "pristine" cloud and rain droplets coming from the melting of ice condensates produced a significant amount of rain between 150 and 210 minutes model time as seen in Figure 4. The accumulated precipitation over the entire domain was 286 mm for the “pristine” and 215 mm for the “hazy” case. Most of this difference can be attributed to the inhibition of precipitation during the early stages of cloud development as illustrated in Figure 5. Cloud structure was also very different between the two simulations. This is clearly shown in Figure 3; two separate cloud systems were still distinct after 170 minutes of simulation for the “pristine” case while during the “hazy” case the two clouds had merged to one cell. The merged system contained increased amounts of ice elements and continued precipitating with slower rates until the end of the simulation. Melting of ice hydrometeors enhanced precipitation for the “pristine” clouds after the system is well developed (Figure 4).

The impact of gigantic cloud condensation nuclei (GCCN) is also important for cloud processes and precipitation (Teller and Levin, 2006; van den Heever et al., 2006). When aerosol sizes are comparable to cloud droplet size - which is often the case for dust and sea-salt, kinetic limitations are imposed on cloud nucleation processes (Barahona et al., 2010). Neglecting such effects may result in significant overestimation of activated cloud droplet number and in reduction of precipitation rates. Nucleation of GCCN is parameterized in the model according to Barahona et al., (2010). In order to examine the impact of GCCN on precipitation, we performed another couple of tests by adding a third coarser mode to the aerosol distribution. The third mode was assumed to have a median diameter of 10μm a standard deviation of 2 and a total concentration of 5 cm^{-3}. Adding GCCN to a hazy environment limited the number of cloud droplets that nucleated and as seen in Figure 6b the rainfall during the early stages of cloud development was increased. In contrary, GCCN did not change significantly the warm stage precipitation for the pristine environment (Figure 6a) because the clean clouds have some large CCN anyhow and the small number of CCN makes them all grow fast.

Cloud processes are of course sensitive to several other model parameters and there are more combinations of cases that could be performed. However, these results are always limited to calculations of single idealized clouds and do not represent real conditions. For example, by adding topographic effects in a 3-D model configuration that is equivalent to the 2-D “pristine” and “hazy” model simulations resulted in substantially different spatial distribution of precipitation as shown in Figure 7. During these simulations, all model parameters remained unchanged except the surface features (topography in this case). The same initial conditions as in previous runs were used (Figure 1) and a western flow with initial wind speed of 3 ms^{-1} was considered for all runs. The impact of topography on precipitation was investigated for three cases, namely “flat terrain”, “idealized hill” and “complex hilly area”. The first case (flat terrain) considers no topographic features and uniform landscape (soil and vegetation classes). In this case, atmospheric stability and cloud microphysics are the governing factors for the evolution of the cloud system. As seen in Figures 7a, b, most of the precipitation was distributed over the western side of the domain for both “pristine” and “hazy” clouds but with different maxima (“pristine” case gave more precipitation). For the second run (“the idealized hill”) the landscape remains the same as in the previous case but a 290 m high ridge with a N-S uniform orientation is added at the center of the domain. The combination of microphysics and cloud dynamics due to mechanical elevation over the hill resulted in a substantially different precipitation pattern that is shown in Figures 7c, d. The distribution of precipitation for this case is clearly related to the location of the hill with more rain falling over the downwind area at the eastern part of the domain. Finally, the third case includes also the same landscape but the topography is representative of a complex hilly area. As illustrated in Figures 7e, f, these topographic features resulted in a completely different distribution of precipitation. Such results indicate that the synergetic effects between the microphysical and macrophysical parameters that contribute in cloud and precipitation processes should be taken into account in relevant modeling studies on a combined way. Otherwise, the results may be misleading when compared to real atmospheric conditions. For example, the “pristine” cases produced overall more precipitation than the “hazy” ones but the distribution of precipitation was found to be much more sensitive to terrain variability than to any of the variations in aerosol properties.

The next section will focus on the use of ICLAMS in a fully coupled mode of air quality and meteorology for a specific test case at the regime of Eastern Mediterranean. The FNS explicit cloud droplets nucleation scheme of the model is used to provide an extra link between cloud processes and prognostic airborne particles, such as mineral dust, sea-salt, sulphates and nitrates.

3.2 Case study

We focus on a case study that combines a low pressure system and a dust storm over the eastern Mediterranean. On 28 January 2003, a cold cyclone moved from Crete through Cyprus accompanied by a cold front. A second air mass transported dust particles from NE Africa towards the coast of Israel and Lebanon. The two air masses interacted over the sea, triggering deep convection as illustrated in Figure 8. These clouds moved northeasterly and on 29 January 2003, heavy rain and hail dispersed over the East Mediterranean coastline and a few kilometres inland. Flood events and agricultural disasters were reported. A detailed analysis and airborne measurements of this episode were obtained during the Mediterranean Israeli Dust Experiment (MEIDEX) as described in Levin et al., 2005. Several runs have been performed for this case. Special attention was given to the amount of available airborne particles that could act as CCN and GCCN for each particular case, examining both the effects on the precipitation reaching the ground and also the effects on the microphysical structure inside the clouds. Modelling results are compared to ground and aircraft observations and some of the findings are discussed here.

The model was configured with three nested grids (15km, 3km and 750m) as seen in Figure 9 and with 32 vertical levels starting from 50m above ground and stretching up to 18km with a geometric ratio of 1.2. For the initial and boundary conditions, a high resolution reanalysis dataset was used. This dataset has been prepared with the Local Analysis and Prediction System (LAPS) (Albers, 1995; Albers et al., 1996). LAPS is a fully integrated, meso-β-scale data assimilation and analysis system designed to handle all types of meteorological observations. It uses an effective analysis scheme to harmonize data of different temporal and spatial resolutions on a regular grid. LAPS surface and upper air fields can then be used as initial and boundary conditions in local forecast models. The prepared dataset includes 24 years of reanalysis (1986-2009) with a grid resolution of 15×15 km and temporal intervals of 3 hours. It is based on the ECMWF operational analysis dataset (with resolution of 0.5×0.5 degrees as initial guess fields and the utilization of all available surface and upper air measurements. The sea surface temperature (SST) used is the NCEP 0.5°×0.5° analysis. During the simulation experiments, two main dust sources were identified: One is located at North East Libya (Gulf of Sidra) and the second at North West

Egypt (Qattara Depression). These areas are illustrated in Figure 9. The chemical properties of dust particles are associated with their origin and with the chemical transformations that occur during their atmospheric lifetime. Aged dust clouds include particles that are coated with sea-salt or sulfates that increase their hygroscopicity and CCN efficiency (Levin et al., 1996, Bougiatioti et al., 2009).

Consistent with Levin et al., (2005), the aerosol particles within the lowest two kilometers of the atmosphere were a mixture of dust and sea-salt. As illustrated in the 3D model plots of Figure 10, dust and sea-salt particles were present all along the frontal line, near the cloud base and the clouds that were formed in this area were highly affected by this increased aerosol concentrations. The south-to-north and west-to-east vertical cross sections of Figure 11 indicate that the dust particles did not elevate higher than two kilometers in the atmosphere and coexisted with sea-salt spray particles along their transportation path. The location of the cross sections is shown in Figure 9.

The number concentration of modelled dust and sea salt particles was tested against in-situ aircraft observations that were performed (between 7:30 and 9:30 UTC) at various heights inside the dust-storm area. Detailed information about the aircraft instrumentation, the sampling and averaging techniques and the variability in particle measurements is provided in Levin et al., (2005). According to their description, the aircraft was flying with a constant speed of 70 m s^{-1} and covered a distance of about 125 kilometres inside the stormy area. Two optical particle counters were used for the measurements of the aerosol size distributions and concentrations. The first was used for aerosols between 0.1-3 μm in diameter and the second for aerosols between 2-16 μm in diameter. Measurements were performed in an irregular manner along the aircraft path and each sampling period lasted for five minutes. For the current work, the average concentration of natural particles for each measurement point is compared towards the corresponding model results. In order to co-locate the aircraft measurements with the appropriate model grid point we considered the average location along the aircraft track. The simulated dust and salt concentrations for the corresponding location in the model is then calculated as the weighted average from the eight nearest model grid points. The concentrations of modelled particles inside the dust layer are in satisfactory agreement with airborne measurements as illustrated in Figure 12, with a correlation coefficient R=0.89. These results indicate that the model is able to reproduce the horizontal and vertical structure of the dust storm qualitatively and quantitatively. The ability of the model to capture these features is important for the next steps of the experiment, since the estimated particles contribute to the cloud droplet nucleation mechanism. As seen in Figure 13, the dust storm is approaching the coast of East Mediterranean from south-west during the morning of 28 January 2008. The clouds that were formed in this area were affected by the dust storm and also by the increased sea salt production due to the relatively strong winds and wind shear. The coexistence of salt and dust particles at heights below cloud base provided significant amounts of highly hygroscopic mixed particles. These clouds contained increased numbers of cloud droplets and moved north-northeast towards the Israel and Lebanon coast. Most of the precipitation from these clouds fell after they reached land and the peak rain rates were reported on the morning of 29 January 2003 around Haifa and North Israel.

Three different scenarios related to the properties of the aerosol particles during the model runs are discussed here. All model parameters were held constant except the percentage of dust particles containing soluble material, thus becoming effective CCN. In experiment 1 (EXP1), 5% of dust particles were hygroscopic while for experiment 2 (EXP2), this percentage was increased to 20%. DeMott et al. (2003a), found that during intense dust episodes, the concentration of ice nuclei (IN) was increased by 20-100 times compared to non-dust environment. Following this approach, EXP3 incorporated 5% hygroscopic dust while the concentration of IN in the model was multiplied by a factor of ten in the presence of mineral dust. The hygroscopic dust particles were assumed to contain 33% sea-salt, as in Levin et al., (2005) where the airborne measurements were analyzed. The aerosol spectrum was fitted in a 3-modal lognormal distribution. The first mode corresponds to particles of mineral dust origin while the other two correspond to sea-salt accumulation and coarse modes, respectively. The median diameter and standard deviation for the accumulated salt mode is 0.36 μm and 1.8 respectively. For the coarse salt mode the median diameter is 2.85 μm and the standard deviation is 1.9. However, dust particles may range from small submicron diameters (away from the sources and at high atmospheric levels) up to GCCN sizes (near sources and at low atmospheric levels). In order to represent this kind of inhomogeneous spatial distribution, the median diameter and standard deviation for the dust mode are estimated from the relative prognostic concentrations of the eight dust bins according to Schultz et al. (1998).

Increasing the percentage of hygroscopic dust particles from 5% to 20% increased also the concentration of small liquid droplets inside the cloud. This resulted in lower autoconversion rates of cloud to rain droplets and significant amount of water was transferred above freezing level. The EXP2 clouds reached higher tops, included more ice water content and the initiation of rainfall was in general delayed by almost 1 hour. In Figure 14, the less polluted cloud (EXP1) reached the maximum top at 9:00 UTC. The EXP2 cloud extended much higher (about 3km higher than EXP1), contained more ice, and eventually produced more rain (one hour later than EXP1; 10:00 UTC instead of 9:00 UTC). The EXP3 cloud also exhibited significant vertical development, with a structure and precipitation amounts similar to that of EXP2. Mineral dust particles affect the microphysical structure of the clouds by acting both as CCN, GCCN and IN and also they interact with cloud dynamics. As illustrated in Figure 15a for the EXP2 case, there was significant convective activity over Haifa at 8:20 UTC on 29 January and the convective available potential energy (CAPE) was 1027 J. When CAPE is large enough, significant amounts of liquid condensates may thrust into the upper levels of a cloud and eventually freeze in higher altitudes. The released latent heat invigorates convection at higher levels. As seen in Figure 15b, a significant amount of liquid condensates were transported above the freezing level. The release of latent heat due to the glaciation of these supercooled droplets had as a result the increase of equivalent potential temperature. This procedure is evident at Figure 15c and is indicated with the arrow pointing the area of increased equivalent potential temperature. After 10 minutes, strong updrafts reached up to 8 kilometers height and transferred condensates to the upper cloud layers as illustrated in Figure 15d. These condensates interact with the available IN in this area of the cloud for the formation of ice particles through heterogeneous icing processes. Thus, increasing the percentage of hygroscopic mineral dust or increasing the IN by an order of magnitude resulted in enhancement of ice particles formation and therefore release of latent heat at higher levels. These interactions between aerosols and cloud dynamics produce clouds with stronger updrafts that reach higher tops and finally produce heavier rainfall.

In order to examine the sensitivity of accumulated precipitation to aerosol properties, we performed a total of nine scenarios with the same model configuration but changing the chemical composition of airborne particles. The physio-chemical characteristics used on each run are shown in Table 4. The first run was performed with the original RAMS model and we call it “control run”. For Case2, only particles-radiation interaction was enabled. For cases three and four, the FNS cloud nucleation parameterization was enabled using the prescribed “pristine” and “hazy” air mass types as in section 3.1. For the next four runs, particle concentration was a prognostic variable and the cloud nucleation scheme was used in an explicit way. The percentage of hygroscopic dust was set to be one (1%), five (5%), ten (10%) and thirty per cent (30%) respectively. For Case 9, we considered five (5%) hygroscopic dust and also the IN concentration was increased by a factor of ten similar to Levin et al., (2005). The modelled 24-hour accumulated precipitation on 29 January 2003 for all nine cases was tested against ground measurements from 86 measuring stations over North Israel.

The model bias score (see Appendix) was calculated for nine thresholds of accumulated precipitation, namely 0.5 mm, 2 mm, 4 mm, 6 mm, 10 mm, 16 mm, 24 mm, 36 mm and 54 mm. The results for each case and each precipitation threshold are shown in Figure 16. Biases equal to one mean that the particular precipitation threshold was simulated as often as observed. Bias below unity indicates model underprediction and bias over one indicates overprediction. The limited time period of the study and the relevant small number of measuring stations (especially at high thresholds) does not allow extracting robust statistical results. However, as seen in Figure 16, the accumulated precipitation was found to be very sensitive to variations of the percentage of dust particles that can be activated as CCN and IN. These results indicate the need for a proper treatment of the links and feedbacks between cloud and aerosol processes. Model results with prognostic aerosol treatment were in general closer to the observations than those of the control run and the model bias for these cases was improved by almost 40% for some thresholds especially at medium and high precipitation heights. Also, assuming a constant prescribed air mass type as in cases three and four, did not improve the model results. The average bias for all thresholds was calculated for each one of the nine cases (see Appendix for definition) and is illustrated in Figure 17. The significant variability in model results that is related to aerosol properties is indicative of their role in atmospheric processes. Cases one to four exhibited more or less the same statistical performance that is probably explained from the use of constant prescribed air mass properties for these runs. However, including the radiative dust effects (Case2) slightly improved the model bias. During the eighth case, the accumulated precipitation field was clearly underestimated due to the increased concentration of hygroscopic particles for this case. Increasing the number of CCN delayed the initiation of precipitation and resulted in the enhancement of ice concentrations. These ice crystals did not grow much because of the lack of water drops at higher levels. Most of these clouds evaporated before they managed to precipitate and the accumulated precipitation was underestimated. The model results were significantly improved for the remaining prognostic aerosol cases (five, six, seven and nine) with average biases of 0.84, 0.84, 0.96 and 0.94 respectively. These findings imply that a more detailed representation of the atmospheric composition and of the aerosol - cloud – radiation feedbacks can provide some insight in the processes involved in the formation of clouds and precipitation and also improve the model performance.

4 Concluding remarks

Aerosol partitioning (anthropogenic/natural) and perturbations on it, such as aging particles, have significant impacts on cloud structure and spatial and temporal distribution of precipitation. Therefore, there is a need for quantification of this forcing at the regional scale since the impacts mentioned above have significant feedbacks with net results not easily quantified. There is still significant amount of uncertainty regarding the aerosol – cloud interaction mechanisms and especially the formation of IN. Therefore there is a need for extensive regional, mesoscale and microscale model simulations with detailed physical and chemical parameterization together with detailed cloud microphysics in order to understand some of the links and feedbacks between air quality and meteorology.

Several sensitivity tests were performed with an integrated atmospheric model that includes online parameterization of aerosol processes, aerosol-radiation interaction, explicit cloud droplet activation scheme and a complete microphysics package. Two-dimensional tests for an idealized case of cloud development indicated a significant response of cloud processes and precipitation to the variations of aerosol number concentration and also to the size distribution of the particles. “Hazy” clouds suspended precipitation while “pristine” clouds precipitated faster and produced more rain that is in agreement with earlier publications. However, in order to simulate the aerosol effects in an approach that is closer to real atmospheric conditions, it is necessary to take also into account the synergetic effects between the various microphysical and macrophysical processes. For example, the distribution of accumulated precipitation was found to be much more sensitive to topographic variations than to aerosol number concentration and/or composition.

A second application for a specific event of dust transportation and convective activity over Eastern Mediterranean, illustrated that this kind of regional modeling approach can be very useful in reproducing many of the important features of aerosol and cloud processes. These findings can be summarized as follows:

1. The meteorological conditions during this particular event and the aerosol field properties were reproduced in the model in satisfactory agreement with observations. This is also indicated by the correlation factor of 0.89 between modelled aerosol concentrations and airborne measurements.
2. An increase of 15% in the concentration of soluble dust particles produced clouds that extended about three kilometres higher and the initiation of precipitation was delayed by almost one hour.
3. Variations between 1-30% in the amount of dust particles that were assumed to contain soluble material resulted in significant changes in cloud properties. The associated variations in the precipitation bias score were up to 80% for some thresholds.
4. In general, online treatment of dust and salt particles as prognostic CCN, GCCN and IN improved the average bias score for the 24h accumulated precipitation by almost 7% in comparison to the runs considering a uniform atmospheric composition all over the domain.

These results illustrate the highly non-linear response of precipitation to aerosol properties and indicate that a large portion of uncertainty remains unresolved. This study focuses mostly on investigating the mechanisms that are associated with the aerosol cloud interactions for a specific event. Therefore it is not possible to extract generic results. Nevertheless, this work represents one of the first limited area modelling studies for aerosol-cloud-radiation effects at the area of Eastern Mediterranean and could be used as a base for future improvements and longer term studies. The role of dust for the weather in Mediterranean is important since dust particles are almost always present at the area and also interact with other natural or anthropogenic pollutants. Especially the role of dust in the distribution of precipitation is more important over areas that suffer from long drought periods such as the Middle East. More intense combined modeling and observational surveys on the interactions between airborne particles and cloud processes at regional and local scale are necessary in order to improve our knowledge on the interactions between atmospheric chemistry and meteorology.

Acknowledgments

This work has been supported by the European Union 6th Framework Program CIRCE IP, contract# 036961 and EUROCONTROL Research Studentship Agreement no CO6/22048ST.

APPENDIX

For each model scenario (Cases 1-9) and for each precipitation threshold a contingency table is constructed as follows (Wilks 2006):

		Observed	
		Yes	No
Modeled	Yes	a	b
	No	c	d

The *a* model-observation pairs mean that both model and observation are over the specific threshold and are usually called hits. Similarly, *b* pairs mean that the model is over the threshold but observation is below it and are called false alarms; *c* pairs mean that the observation is over the threshold but the model is below it and are called misses and *d* pairs mean that both model and observation are below the threshold for a station and are called correct rejections.

The total number of hits (*a*), false alarms (*b*) and misses (*c*) for each threshold are then used to calculate the MODEL BIAS (B):

$$B = \frac{a+b}{a+c}$$

Unbiased forecasts exhibit bias=1, while bias greater than one indicates overprediction and bias less than one indicates underprediction.

The AVERAGE BIAS ($\overline{B}$) for all precipitation thresholds is calculated as:

$$\overline{B} = \frac{1}{N}\sum_{i=1}^{i=N} B(i),$$

Where *B(i)* is the bias for each specific threshold and N is is the total number of precipitation thresholds.

REFERENCES

Albers, S. C.: The LAPS wind analysis, Weather and Forecasting, 10, 342-352., 1995.

Albers, S., McGinley, J. A., Birkenheuer, D. and Smart, J.R: The Local Analysis and Prediction System (LAPS): Analysis of clouds, precipitation, and temperature, Weather and Forecasting, 11, 273-287, 1996.

Albrecht, B. A.: Aerosols, cloud microphysics, and fractional cloudiness, Science 245, 1227-1230, 1989.

Alfaro, S.C. and Gomes, L.: Modeling mineral aerosol production by wind erosion: emission intensities and aerosol size distributions in source areas, Journal of Geophysical Research 106 (D16), pp. 18075–18084, 2001.

Andreae, M. O., Charlson R. J., Bruynseels F., Storms H., van Grieken, R. and Maenhaut W.: Internal mixtures of sea salt, silicates and excess sulfate in marine aerosols, Science, 232, 1620-1623, 1986.

Andreae, M. O. and Rosenfeld, D.: Aerosol-cloud-precipitation interactions, Part 1, The nature and sources of cloud-active aerosols, Earth Science Reviews, 89, 13–41, 2008.

Astitha, M. and Kallos, G.: Gas-phase and aerosol chemistry interactions in South Europe and the Mediterranean Region, Env. Fl. Mech.,doi:10.1007/s10652-008-91107.,2008.

Astitha, M., Kallos, G., Spyrou, C., O'Hirok, W., Lelieveld, J., and Denier van der Gon, H. A. C.: Chemically aged and mixed aerosols over the Central Atlantic Ocean – potential impacts, Atmos. Chem. Phys. 10, 5797-5822, 1020 doi:10.5194/acp-10-5797,2010.

Barahona, D., West, R. E. L., Stier, P., Romakkaniemi, S., Kokkola, H., and Nenes, A.: Comprehensively accounting for the effect of giant CCN in cloud activation parameterizations, Atmos. Chem. Phys., 10, 2467–2473, 2010.

Bougiatioti, A., Fountoukis, C., Kalivitis, N., Pandis, S.N., Nenes, A. and Mihalopoulos, N.: Cloud Condensation Nuclei Measurements in the Marine Boundary Layer of the Eastern Mediterranean: CCN closure and droplet growth kinetics, Atmos.Chem.Phys., 9, 7053-7066, 2009.

Charlson, R. J., Langner, J., Rodhe, H.: Sulphate aerosol and climate, Nature, 348, 22, 1990.

Charlson, R. J., Schwartz, S. E., Hales, J. M., Cess, R. D., Coakley, J. A. , Hansen J. E. and D. J. Hofmann: Climate forcing by anthropogenic aerosols, Science, 255, 423-430, 1992.

Charlson R. J., Seinfeld, J. H., Nenes, A., Kulmala, M., Laaksonen, A., Facchini, M. C.: Reshaping the Theory of Cloud Formation, Science, 292, 2025-2026, 2001.

Chen, C., and Cotton, W. R.: A one-dimensional simulation of the stratocumulus-capped mixed layer, Bound.-Layer Meteor., 25, 289-321, 1983

Chung, S. H., and Seinfeld, J. H.: Global distribution and climate forcing of carbonaceous aerosols, J. Geophys. Res., 107(D19), 4407, doi:10.1029/2001JD001397, 2002.

Cotton W. R., Pielke, R. A. Sr., Walko, R. L., Liston, G. E., Tremback, C. J., Jiang, H. , McAnelly, R. L., Harrington, J. Y., Nicholls, M. E., Carrio, G. G. and J. P. Mc Fadden: RAMS 2001: Current status and future directions, Meteoro. and Atmos Phys 82, 5-29, 2003.

Cotton, W.R., Zhang, H., McFarquhar, G.M. and S.M. Saleeby: Should we consider polluting hurricanes to reduce their intensity?, J. Wea. Mod., 39, 70-73, 2007.

DeMott, P. J., Sassen, K., Poellet, M. R., Baumgardner, D., Rogers, D. C., Brooks, S. D., Prenni, A. J. and Kreidenweis, S. M.: African dust aerosols as atmospheric ice nuclei, Geophys. Res. Lett. 30 (14), 1732, doi:10.1029/2003GL017410, 2003a.

Davies, H.C.: Limitations of some common lateral boundary schemes used in regional NWP models, Mon Wea Rev 111: 1002–1012, 1983.

DeMott, P. J., Sassen, K., Poellet, M. R., Baumgardner, D., Rogers, D. C., Brooks, S. D., Prenni, A. J. and Kreidenweis, S. M.: African dust aerosols as atmospheric ice nuclei, Geophys. Res. Lett, 30.1732, doi: 10.1029/2003GL017410, 2003.

Dockery, D. W. and Pope, C. A.: Acute respiratory effects of particulate air pollution, Annu. Rev. Publ. Health, 15, 107–132, 1994.

Fécan, F., Marticorena, B., and Bergametti, G.: Parameterization of the increase of the Aeolian erosion threshold wind friction velocity due to soil moisture for arid and semi-arid areas, Annales de Geophysique, 17, 149 – 157, 1999.

Fountoukis, C. and Nenes, A.: Continued Development of a Cloud Droplet Formation Parameterization for Global Climate Models, J. Geophys. Res.,110, D11212, 2005.

Fountoukis, C., Nenes, A., Meskhidze, N., Bahreini,, R., Conant, W. C., Jonsson, H., Murphy, S., Sorooshian, A., Varutbangkul, V., Brechtel, F., Flagan, R. C.,.and Seinfeld, J. H.: Aerosol - cloud drop concentration closure for clouds sampled during the International Consortium for Atmospheric Research on Transport and Transformation 2004 campaign, J. Geophys. Res., 112, D10S30, doi:10.1029/2006JD007272, 2007.

Fu, Q. and Liou, K.N: On the correlated k-distribution method for radiative transfer nonhomogeneous atmosphere, J. Atmos. Sci. 49 , pp. 2139–2156, 1992.

Gong, S. L, Barrie, L. A. and. Lazare, M.: Canadian Aerosol Module (CAM): a size-segregated simulation of atmospheric aerosol processes for climate and air quality models. 2. Global sea-salt aerosol and its budgets, Journal of Geophysical Research 107, D24, 4779, 2002.

Gong, S. L.: A parameterization of sea-salt aerosol source function for sub- and super-micron particles, Global Biogeochemical Cycles 17 (4), p. 1097, 2003.

Grini, A., Zender, C. S., and Colarco, P. R.: Saltation sandblasting behavior during mineral dust aerosol production, Geophys. Res. Lett., 29.1868, doi:10.1029/2002GL015248, 2002.

Harrington, J. Y.: The Effects of Radiative and Microphysical Processes on Simulated Warm and Transition Season Arctic Stratus., Ph.D. Thesis, Colorado State University, Ft. Collins, CO. 298pp, 1997.

Herut, B., Collier, R., and Krom, M.D.: The role of dust in supplying nitrogen and phosphorus to the Southeast Mediterranean, Limnology and Oceanography 47 , pp. 870–878, 2002.

Hill, G. E.: Factors controlling the size and spacing of cumulus clouds as revealed by numerical experiments, J Atmos Sci 31: 646, 1974.

Iacono, M. J., Mlawer, E. J., Clough, S. A. and Morcrette, J. J.: Impact of an improved longwave radiation model, RRTM, on the energy budget and thermodynamic properties of the NCAR Community Climate Model, CCM3. J. Geophys. Res., 105:14873–14890, 2000.

IPCC: Climate Change 2001: Mitigation. Intergovernmental Panel on Climate Change (IPCC), B. Metz, et al. (eds), Cambridge University Press, Cambridge, UK., 2001a.

IPCC: Climate Change 2001: Impacts, Adaptation, and Vulnerability. Intergovernmental Panel on Climate Change (IPCC), J.J. McCarthy, et al. (eds.),Cambridge University Press, Cambridge, UK, 2001b.

IPCC: Changes in atmospheric constituents and radiative forcing: Climate change 2007: the physical science basis, Cambridge University Press, New York, USA, and Cambridge, UK, 2007.

Jacobson, M. Z.: Global direct radiative forcing due to multicomponent anthropogenic and natural aerosols, J. Geophys. Res., 106,1551–1568, 2001.

Junkermann, W., Hacker, J., Lyons, T., and Nair, U.: Land use change suppresses precipitation, Atmos. Chem. Phys., 9, 6531–6539, 2009

Kallos, G., Papadopoulos, A., Katsafados, P. Nickovic, S.: Trans-Atlantic Saharan dust transport: Model simulation and results, J. Geophysical Research, 111, D09204, doi: 10.1029/2005JD006207, 2006

Kallos, G., Astitha, M., Katsafados, P. and Spyrou, C.: Long-Range Transport of Anthropogenically and Naturally Produced particulate matter in the Mediterranean and North Atlantic: Current State of Knowledge, J. of Applied Meteorology and Climatology 46, (8): 1230-1251. doi 10.1175/JAM2530.1, 2007.

Karyampudi, V. M.: A detailed synoptic-scale study of the structure, dynamics, and radiative effects of the Saharan air layer over the eastern tropical Atlantic during GARP Atlantic Tropical Experiment, M. S. thesis, Department of Meteorology, The Pennsylvania State University, 136 pp., 1979.

Karyampudi, V. M., Palm, S. P., Reagen, J. A., Fang, H., Grant, W. B., Hoff, R. M., Moulin, C., Pierce, H. F., Torres, O., Browell, E. V. and Melfi, S. H.: Validation of the Saharan dust plume conceptual model using lidar, Meteosat, and ECMWF data, B. Am. Meteor. Soc., 80, 1045–1075, 1999.

Krichak, S. O. and Levin, Z.: On the cloud microphysical processes during the November 2, 1994, hazardous storm in the southeastern Mediterranean as simulated with mesoscale model, Atmos. Res., 53:63–89, 2000.

Klemp J. B, Wilhelmson, R. B.: The simulation of threedimensional convective storm dynamics, J Atmos Sc. 35: 1070–1096, 1978.

Köhler, H.: The nucleus in and the growth of hygroscopic droplets, Trans. Faraday Soc., 32, 1151–161, 1936.

Lacis, A. A., and Oinas, V.: A description of the correlated k distributed method for modeling nongray gaseous absorption, thermal emission, and multiple scattering in vertically inhomogeneous atmospheres, J. Geophys. Res., 96, 9027-9063, doi: 10.1029/90JD01945, 19, 1991.

Leeuw, G., Neele, F. P., Hill, M., Smith, M. H. and Vignali, E.: Production of sea spray aerosol in the surf zone, Journal of Geophysical Research—Atmospheres 105, pp. 29397–29409, 2000.

Levin, Z., Ganor, E. and Gladstein, V.: The effects of desert particles coated with sulfate on rain formation in the eastern Mediterranean, J. Appl. Meteorol., 35, 1511-1523, 1996.

Levin, Z., Teller, A., Ganor, E., and Yin, Y.: On the interactions of mineral dust, sea-salt particles and clouds: A measurement and modeling study from the Mediterranean Israeli Dust Experiment campaign, J. Geophys. Res., 110, D20202, doi: 10.1029/2005JD005810, 2005.

Levin, Z. and Cotton, W. R.: Aerosol Pollution Impact on Precipitation-A Scientific Review, Springer, 386 pp., ISBN:978-1-4020-8689-2, 2009.

Lilly, D. K.: On the numerical simulation of buoyant convection, Tellus XIV: 148–172, 1962.

Lohmann, U., and Feichter, J.: Global indirect aerosol effects: A review, Atmos. Chem. Phys., 5, 715–737, 2005.

Lu, H. and Shao, Y.: A new dust model for dust emission by saltation bombardment, J. Geophys. Res., 104, 16827-16841, 1999.

Lynn, B., Khain, A., Dudhia, J., Rosenfeld, D., Pokrovsky, A. and Seifert, A.: Spectral (bin) microphysics coupled with a mesoscale model (MM5). Part 2: Simulation of a CaPe rain event with squall line. Mon. Wea. Rev., 133, 59-71, 2005b.

Mahrer, Y., Pielke, R. A.: A numerical study of the airflow over irregular terrain, Contributions to Atmospheric Physics 50: 98–113, 1977.

Mahowad, N., Jickells, T. D. , Baker, A. R., Artaxo, P., Benitez-Nelson, C. R., Bergametti, G., Bond, T. C., Chen, Y., Cohen, D. D., Herut, B., Kubilay, N., Losno, R., Maenhaut, C. L. W., McGee, K. A., Okin, G. S., Siefert, R. L. and Tsukuda, S.: Global distribution of atmospheric phosphorus sources, concentrations and deposition rates, and anthropogenic impacts, Global Biogeochem. Cy., 22, GB4026, doi:10.1029/2008GB003240, 2008.

Marticorena, B., and Bergametti, G.: Modeling the atmospheric dust cycle: 1. Design of a soil derived dust emission scheme, Journal of Geophysical Research, 100(D8), 16415 – 16430, 1995.

Marticorena, B., Bergametti, G., Gillette, D., Belknap, J.: Factors controlling threshold friction velocity in semiarid and arid areas of the United States, J. Geophys. Res., 102, 23,277–23,288, 1997a.

Marticorena, B., Bergametti, G., Aumont, B., Callot, Y., Doume, C. N. and Legrand, M.: Modeling the atmospheric dust cycle 2, Simulation of Saharan dust sources, J. Geophys. Res., 102, 4387–4404, 1997b.

Mavromatidis, E. and Kallos, G.: An investigation of cold cloud formation with a 3-D model with explicit microphysics, J. Geophysical Research. doi 2002JD0027111, JGRD, vol. 108, 2003.

Mavromatidis, E., Lekas, T., and Kallos, G.: Analysis of a two-layer cloud system with RAMS model and comparison to airborne observations. Env. Fluid Mech. dio: 10.1007/s10652-007-9043-6. Vol 7, 537-568, 2007.

Mellor, G.L., Yamada, T.: Development of a turbulence closure model for geophysical fluid problems. Rev Geophys Space Phys 20: 851–875, 1982.

Meskhidze, N., Chameides, W. L., Nenes, A., and Chen, G.: Iron mobilization in mineral dust: Can anthropogenic SO2 emissions affect ocean productivity?, Geophys. Res. Lett., 30(21), 2085, doi:10.1029/ 2003GL018035, 2003.

Meskhidze, N., Chameides, W. L., and Nenes, A.: Dust and pollution: A recipe for enhanced ocean fertilization?, J. Geophys. Res., 110, D03301, doi:10.1029/2004JD005082, 2005.

Meskhidze, N. and Nenes, A.: Phytoplankton and Cloudiness in the Southern Ocean, Science, 314, 1419–1423, 2006.

Meyers, M. P., DeMott, P. J. and Cotton, W. R.: New primary ice nucleation parameterizations in an explicit cloud model, J. Appl. Meteor., 31, 708–721, 1992.

Meyers, M. P., Walko, R. L., Harrington, J. Y. and Cotton, W. R.: New RAMS cloud microphysics parameterization. Part II: The two-moment scheme, .Atmos. Res., 45:3–39, 1997.

Mitsakou, C., Kallos, G., Papantoniou, N., Spyrou, C., Solomos, S., Astitha, M., Housiadas, C.: Saharan dust levels in Greece and received inhalation doses, Atmos. Chem. Phys. Disc., 8, 7181-7192, 2008

Mlawer, E. J., Taubman, S. J., Brown, P. D., Iacono, M. J., and Clough, S. A.: Radiative transfer for inhomogeneous atmospheres: RRTM, a validated correlated-k model for the longwave, J. Geophys. Res., 102 (D14) 16663–16682, 1997.

Monahan, E. C., Spiel, D. E. and Davidson, K. L.: A model of marine aerosol generation via whitecaps and wave disruption, Oceanic Whitecaps, E.C. Monahan and G. Mac Niocaill, Eds., D. Reidel, 167-174, 1986.

Myhre, G., Grini, A., Haywood, J. M., Stordal, F., Chatenet, B., Tanr, D., Sundet, J. K. and Isaksen, I. S. A.: Modelling the radiative impact of mineral dust aerosol during the Saharan Dust Experiment (SHADE) campaign, J Geophys Res, 108 (D18), 8579, doi:10.1029/2002JD002566, 2003b.

Nenes, A., and Seinfeld, J. H.: Parameterization of cloud droplet formation in global climate models, J. Geophys. Res., 108, 4415, 2003.

Nenes, A., Charlson, R. J., Facchini, M. C., Kulmala, M., Laaksonen, A., Seinfeld, J.H.: Can Chemical Effects on Cloud Droplet Number Rival the First Indirect Effect?, Geoph.Res.Lett, 29 (17), 1848, doi: 10.1029/2002GL015295, 2002.

Osborne, S. R., Johnson, B. T., Haywood, J. M., Baran, A. J., Harrison, M. A. J. and McConnell C. L.: Physical and optical properties of mineral dust aerosol during the Dust and Biomass-burning Experiment, J. Geophys. Res., 113, D00C03, doi:10.1029/2007JD009551, 2008.

Pérez, C., Nickovic, S., Pejanovic, G., Baldasano, J. M. and Özsoy, E.: Interactive dust-radiation modeling: a step to improve weather forecasts, Journal of Geophysical Research, 111, D16206, doi:10.1029/2005JD006717, 2006.

Pielke, R. A., Cotton, W. R., Walko, R. L., Tremback, C. J., Lyons, W. A., Grasso, L. D., Nicholls, M. E., Moran, M. D., Wesley, D. A., Lee, T. J. and Copeland, J. H.: A comprehensive meteorological modeling system—RAMS, Meteor. Atmos. Phys.,49, 69–91, 1992.

Pierce, J. R. and Adams, P. J.: Global evaluation of CCN formation by direct emission of sea salt and growth of ultrafine sea salt, J. Geophys. Res., 111, D06203, doi:10.1029/2005JD006186, 2006.

Prospero, J. M., and Nees, R. T.: Impact of the North African drought and El Niño on mineral dust in the Barbados trade winds, Nature, 320, 735–738, 1986.

Prospero, J. M.: Long-term measurements of the transport of African mineral dust to the southeastern United States: Implications for regional air quality, J. Geophys. Res., 104, 15,917–15,927, 1999.

Prospero, J. M., Ginoux, P., Torres, O. , Nicholson, S. E. and Gill, T. E.: Environmental characterization of global sources of atmospheric soil dust identified with the NIMBUS 7 Total

Ozone Mapping Spectrometer (TOMS) absorbing aerosol product, Rev. Geophys., 40(1), 1002, doi:10.1029/2000RG000095, 20

Prospero, J. M., Blades, E., Mathison, G. and Naidu, R.: Interhemispheric transport of viable fungi and bacteria from Africa to the Caribbean with soil dust, Aerobiologia 21 (1), pp. 1–19, 2005.

Pruppacher, H. R. and Klett, J. D.: Microphysics of Clouds and Precipitation, Second Revised and Enlarged Edition with an Introduction to Cloud Chemistry and Cloud Electricity, Kluwer Academic Publishers, Dordrecht, 954 pp, 1997.

Querol, X., Pey, J., Pandolfi, M., Alastuey, A., Cusack, M., Perez, N., Moreno, T., Viana, M., Mihalopoulos, N., Kallos, G., Kleanthous, S.: African dust contributions to mean ambient PM10 mass-levels across the Mediterranean Basin Atmospheric Enviroment, Volume 43, Issue 28, Pages 4266-4277, 2009.

Ramanathan, V., Muvva,,V.,Ramana, G., Roberts, G., Kim, D., Corrigan, C., Chung, C., and Winker, D.: Warming trends in Asia amplified by brown cloud solar absorption, Nature, 448, 575–578, 2007

Rosenfeld, D., Khain, A., Lynn, B. and Woodley, W.L.: Simulation of hurricane response to suppression of warm rain by sub-micron aerosols. Atmos. Chem. Phys., 7, 3411-3424, 2007.

Rosenfeld D., Lohmann, U., Raga, G. B., O'Dowd, C. D., Kulmala, M., Fuzzi, S. Reissell, A., Andreae, M. O.:Flood or Drought: How Do Aerosols Affect Precipitation?, ScienceVol. 321. no. 5894, pp. 1309 – 1313 doi: 10.1126/science.1160606, 2008.

Sassen, K., DeMott, P. J., Prospero, J. M. and Poellet, M. R.: Saharan dust storms and indirect aerosol effects on clouds: CRYSTAL-FACE results, Geophys. Res. Lett, 30.1633, doi:10.1029/2003GL017371, 2003.

Saleeby, S. M. and Cotton, W.R.: A large droplet mode and prognostic number concentration of cloud droplets in the Colorado State University Regional Modeling System (RAMS). Part I: Module descriptions and supercell test simulations, J. Appl. Meteor., 43, 182-195, 2004.

Sehmel G.A.: Particle and gas dry deposition: A review, Atmospheric Environment 14, pp. 983–1011, 1980.

Seifert, A. and Beheng, K.D.: A two-moment cloud microphysics parameterization for mixed-phase clouds. Part II: Maritime vs. continental deep convective storms, Meteorol. And Atmos. Phys., 92,67-82, 2006.

Seinfeld J. H. and Pandis S. N.: Atmospheric Chemistry and Physics: From Air Pollution to Climate Change, J. Wiley, Sons, Inc., New York, 1998.

Seinfeld, J. H., et al.: ACE-ASIA regional climate and Atmospheric chemical effects of Asian dust and pollution, Bull. Amer. Meteorol. Soc., 85, 367;380, 2004.

Schulz, M., Balkanski, Y., Guelle, W., Dulac, F.: Role of aerosol size distribution and source location in a three-dimension simulation of a Saharan dust episode tested against satellite-derived optical thickness, J Geophys Res-Atmosphere 103: 10,579-10,592, 1998.

Slinn, S. A. and Slinn, W. G. N.: Predictions for particle deposition on natural waters, Atmospheric Environment 14, pp. 1013–1016, 1980.

Smagorinsky, J.: General circulation experiments with the primitive equations. Part I: The basic Experiment, Mon Wea Rev 91: 99–164, 1963.

Spyrou, C., Mitsakou, C., Kallos, G., Louka, P., and Vlastou, G.: An improved limited-area model for describing the dust cycle in the atmosphere, J. Geophys. Res., doi: 10.1029/2009JD013682, 2010.

Stevens, B. and Feingold, G.: Untangling aerosol effects on clouds and precipitation in a buffered system, Nature, 461, doi:10.1038/nature08281, 2009.

Teller, A. and Levin, Z.: The effects of aerosols on precipitation and dimensions of subtropical clouds; a sensitivity study using a numerical cloud model, Atmos. Chem. And Phys. 6, 67–80, 2006

Tremback, C. J.: Numerical simulation of a mesoscale convective complex: Model development and numerical results, PhD Diss., Atmos Sci Paper No 465, Colorado State University, Department of Atmospheric Science, Fort Collins, CO 80523, 1990.

Twomey, S.: The influence of pollution on the short-wave albedo of clouds, J. Atmos. Sci. 34, 1149-1 152, 1977.

Van den Heever, S. C., Carrio, G. G., Cotton, W. R., DeMott, P. J. and Prenni, A. J.: Impacts of nucleating aerosol on Florida storms: Part I: Mesoscale simulations, J. Atmos. Sci., 63, 1752–1775, 2006.

Van den Heever, S., and Cotton, W. R.: Urban aerosol impacts on downwind convective storms, J. Appl. Met., 46, 828-850, 2007.

Walko, R. L., Band, L. E., Baron, J., Kittel, T. G. F., Lammers, R., Lee, T. J., Ojima, D., Pielke, R. A. Sr, Taylor, C., Tague, C., Tremback, C. J., Vidale, P. J.:Coupled atmosphere-biophysics – hydrology models for environmental modelling, J Appl Meteor 39: 931–944, 2000

Wesely, M. L.: Parameterization of surface resistances to gaseous dry deposition in regional-scale numerical models, Atmospheric Environment, 23, 1293-1304, 1989.

Wurzler, S., Reisin, T. G. and Levin, Z.: Modification of mineral dust particles by cloud processing and subsequent effects on drop size distributions, J. Geophys. Res. 105 , 4501, 2000.

Yin, Y., Wurzler, S., Levin, Z. and Reisin, T. G.: Interactions of mineral dust particles and clouds: Effects on precipitation and cloud optical properties, J. Geophys. Res., 107(D23), 4724, doi:10.1029/2001JD001544, 2002.

Yin, Y. and Chen, L.: The effects of heating by transported dust layers on cloud and precipitation: a numerical study, Atmos. Chem. Phys., 7, 3497-3505, doi:10.5194/acp-7-3497-2007, 2007.

Yu, S., Saxena, V. K., Wenny, B. N., DeLuisi, J. J., Yue, G. K. and Petropavlovskikh, I. V.: A study of the aerosol radiative properties needed to compute direct aerosol forcing in the south-eastern United States, Journal of Geophysical Research 105, pp. 24,739–24,749, 2000.

Wilks, D. S.: Statistical Methods in the Atmospheric Sciences, Academic Press NY, pp 260-271, 2006.

Zender, C. S., Bian, H. and Newman, D.: Mineral Dust Entrainment and Deposition (DEAD) model: Description and 1990s dust climatology, J. Geophys. Res., 108(D14), 4416, doi:10.1029/2002JD002775, 2003

Zender, C. S., Miller, R. and Tegen, I.: Quantifying Mineral Dust Mass Budgets: Terminology, Constraints, and Current Estimates, Eos Trans. AGU, 85(48), 509–512, doi:10.1029/2004EO480002, 2004.

Zhang, K. M., Knipping, E. M., Wexler, A. S., Bhave, P. V. and Tonnesen, G. S. :Size distribution of sea-salt emissions as a function of relative humidity, Atmospheric Environment 39, pp. 3373–3379, 2005

Zhang, H., McFarquhar, G. M., Saleeby, S. M., Cotton, W. R.: Impacts of Saharan dust as CCN on the evolution of an idealized tropical cyclone, Geophys. Res. Lett., 34, L14812, doi:10.1029/2007GL029876, 2007.

Table 1. ICLAMS configuration options. New capabilities (compared to RAMS) are shown in bold.

Basic Equation	• Non hydrostatic time split compressible
Dimensionality	• 2 dimensional • 3 dimensional
Vertical Coordinate	• Standard Cartesian coordinate • Terrain following height coordinate
Horizontal Coordinate	• Rotated polar-stereographic transformation • Lambert conformal transformation
Grid Structure	• Arakawa-C grid stagger • Unlimited number of nested grids • User specified space and time step nesting ratios • Ability to add and subtract nests
Time differencing	• Hybrid combination of leapfrog and forward in time
Turbulence closure	• Smagorinsky (1963) deformation K closure scheme with stability modifications made by Lilly (1962) and Hill (1974) • Deardorff level 2.5 scheme – eddy viscosity as a function of TKE • Mellor-Yamada level 2.5 scheme – ensemble averaged TKE (Mellor and Yamada 1982) • Isotropic TKE parameterizations for high resolution simulations
Cloud microphysics	• Warm rain processes • Five ice condensate species • Two-moment bulk scheme (Walko et al., 1995; Meyers et al.,1997). • **Cloud droplet activation scheme (Nenes and Seinfeld, 2003; Fountoukis and Nenes, 2005)**
Convective Parameterization	• Modified Kuo – Tremback (1990) • Kain-Fritsch cumulus parameterization
Radiation	• Chen and Cotton (1983) long/shortwave model – cloud processes considering all condensate as liquid • Harrington (1997) long/shortwave model – two stream scheme interacts with liquid and ice hydrometeor size spectra and **with dust particles** • **Rapid Radiative Transfer Model (RRTM) (Mlawer et al. 1997, Iacono et al. 2000) with aerosol radiative effects**
Aerosol parameterization	• **Mineral Dust** • **Sea salt spray** • **Anthropogenic aerosols (primary emissions and chemical formation)** • **Dry deposition** • **Wet deposition**
Emissions	• **Anthropogenic emissions (JRC 0.1°x 0.1° global emissions of CO_2, NH_3, CH_4, SO_2, NO_x, CO, N_2O, VOCs, OC & BC)** • **Biogenic emissions (Gunther et al. 1995)** • **Any other emission inventory or combinations of more than one.**
Chemistry parameterization	• **Online calculation of photodissociation rates** • **Online gas, aqueous and aerosol phase chemistry**
Lower boundary	• Soil – vegetation – snow parameterization (LEAF-3) (Walko et al, 2000) • Urban canopy scheme – 3D field of drag coefficients based on building characteristics
Boundary conditions	• Klemp and Wilhelmson (1978) radiative condition • Large-scale nudging boundary conditions Davies (1983) • Cyclic or periodic boundaries
Initialization	• Horizontally homogeneous from a single sounding • RAMS/ISAN package – hybrid isentropic terrain following analysis using gridded larger scale model data (ECMWF, NCEP) combined with a variety of observed data types Tremback (1990) • **LAPS 3-D data assimilation pre-processing system**
Data Assimilation	• 4-D analysis nudging to data analysis • Observational data nudging scheme based on 'direct' nudging to the observations

Table 2. Land cover and vegetation type as categorized in LEAF3 scheme

Category number	Vegetation type
0	Ocean
1	Lakes, rivers, streams
2	Ice cap/glacier
3	Desert, bare soil
4	Evergreen needleleaf tree
5	Deciduous needleleaf tree
6	Deciduous broadleaf tree
7	Evergreen broadleaf tree
8	Short grass
9	Tall grass
10	Semi-desert
11	Tundra
12	Evergreen shrub
13	Deciduous shrub
14	Mixed woodland
15	Crop/mixed farming, grassland
16	Irrigated crop
17	Bog or marsh
18	Wooded grassland
19	Urban and built up
20	Wetland evergreen broadleaf tree
21	Very urban

Table 3. Hourly accumulated precipitation over all the domain and maximum values for the number concentration and mixing ratio of cloud, rain and pristine-ice condensates, for two air mass type scenarios.

Time after model start (h)	Air mass type scenario	Total accumulated precipitation (mm)	Cloud No concentration [cm^{-3}]	Cloud mixing ratio [$g\ kg^{-1}$]	Rain No concentration [L^{-1}]	Rain mixing ratio [$g\ kg^{-1}$]	Pristine-ice No concentration [L^{-1}]	Pristine-ice mixing ratio [$g\ kg^{-1}$]
2	PRISTINE	84	130	0.76	27.65	0.47	207	0.13
	HAZY	26	2133	0.48	2.20	0.37	444	0.19
3	PRISTINE	74	99	0.08	3.19	0.22	89	0.05
	HAZY	101	1363	0.39	2.47	0.33	115	0.05
4	PRISTINE	98	22	0.05	1.28	0.14	88	0.05
	HAZY	67	592	0.13	2.98	0.09	97	0.06
5	PRISTINE	23	111	0.08	1.85	0.12	81	0.05
	HAZY	20	377	0.44	2.24	0.09	94	0.05
6	PRISTINE	7	97	0.31	2.97	0.08	109	0.06
	HAZY	3	231	0.12	2.04	0.03	74	0.04

Table 4. Model characteristics for nine aerosol scenarios.

Aerosol Cases	**Aerosol-cloud interaction**	**Aerosol-radiation interaction**
Case1 (control run)	NO	NO
Case2 (only radiation interaction)	NO	YES
Case3 (constant air mass – "pristine")	YES	NO
Case4 (constant air mass – "hazy")	YES	NO
Case5 (prognostic air mass - 1% hygroscopic dust)	YES	YES
Case6(prognostic air mass - 5% hygroscopic dust)	YES	YES
Case7 (prognostic air mass - 10% hygroscopic dust)	YES	YES
Case8 (prognostic air mass - 30% hygroscopic dust)	YES	YES
Case9 (prognostic air mass - 5% hygroscopic dust + INx10)	YES	YES

Figure captions

Figure 1: Initial conditions for the thermodynamic profile of the atmosphere.

Figure 2: Distribution of the available aerosol particles.

Figure 3: Total condensates mixing ratio (g kg^{-1}) for the "pristine" (left column) and the "hazy" (right column) scenarios.

Figure 4: Maximum precipitation rate (mm h^{-1}) for the "pristine" and "hazy" air mass scenarios. Values are taken every 10 minutes.

Figure 5: Hourly accumulated precipitation (mm) over the domain, for the "pristine" and "hazy" CCN scenarios.

Figure 6: a) Maximum precipitation rate (mm h^{-1}) for the "pristine" and "pristine+GCCN" air mass scenarios. b) Maximum precipitation rate (mm h^{-1}) for the "hazy" and "hazy+GCCN" air mass scenarios.

Figure 7: 4h accumulated precipitation (colour palette in mm) and 50m topographic line contours. 1st row: "pristine" aerosol. 2nd row: "hazy" aerosol. 1st column: No topography (flat terrain). 2nd column: artificial obstacle vertical to the general flow. 3rd column: complex topography.

Figure 8: a) Cloud cover percentage (greyscale), near surface streamlines (green contours) and dust - load (red contours in mg m^{-2}). ICLAMS valid 28January 2003, 1100 UTC. b) MODIS-Aqua visible channel, on 28 January 2003 1100, UTC.

Figure 9: Dust flux in μg m^{-2} on 27 January 2003 09:00 UTC. Dashed rectangulars indicate the location of the nested domains. Solid lines indicate the locations of the cross sections of Figure 11.

Figure 10: a) Isosurface of 90% relative humidity (blue surface) and dust concentration (μg m^{-3}) over this surface (colour palette), 28 January 2003 12:00 UTC. b) Isosurface of 5 μg m^{-3} sea-salt concentration (blue) coloured with dust concentration over it (colour palette in μg m^{-3}), 28 January 2003 12:00 UTC.

Figure 11: Vertical cross sections of dust concentration (color palette in μg m^{-3}) and sea salt concentration (red line contours in μg m^{-3}).

Figure 12: Comparison of aircraft measurements of natural particles with modeled dust and salt concentrations inside the dust layer (below 2km). The red line indicates the linear regression line while the dotted line indicates the y=x line.

Figure 13: Modeled dust number concentration (cm^{-3}) at 538 m height on 28 January 2003, 09:20 UTC. Dots indicate the locations of the aircraft measurements.

Figure 14: West to East cross-section of rain mixing ratio (color palette in g kg^{-1}) and ice mixing ratio (red line contours in g kg^{-1}) at the time of highest cloud top over

Haifa. a) 9 UTC 29 January 2003 assuming 5% hygroscopic dust (EXP1). b) 10 UTC 29 January 2003 assuming 20% hygroscopic dust (EXP2). c) 9 UTC 29 January 2003 assuming 5% hygroscopic dust and INx10 (EXP3).

Figure 15: a) Modelled thermodynamic profile of the atmosphere over Haifa at 08:20 UTC, 29 January 2003. b) Liquid water mixing ratio (colour palette in g kg^{-1}) and ambient temperature (red contours in C^{o}) (W-E cross-section over Haifa at 08:20 UTC, 29 January 2003). c) Equivalent potential temperature (colour palette in K) and updrafts (black contours in m s^{-1}) (W-E cross section over Haifa at 08:20 UTC, 29 January 2003). d) Equivalent potential temperature (colour palette in K) and updrafts (black contours in m s^{-1}) (W-E cross section over Haifa at 08:30 UTC, 29 January 2003).

Figure 16: Bias of the 24 hours accumulated precipitation for 86 stations and for nine scenarios of aerosol composition.

Figure 17: Average bias of the 24 hours accumulated precipitation for nine scenarios of aerosol composition.

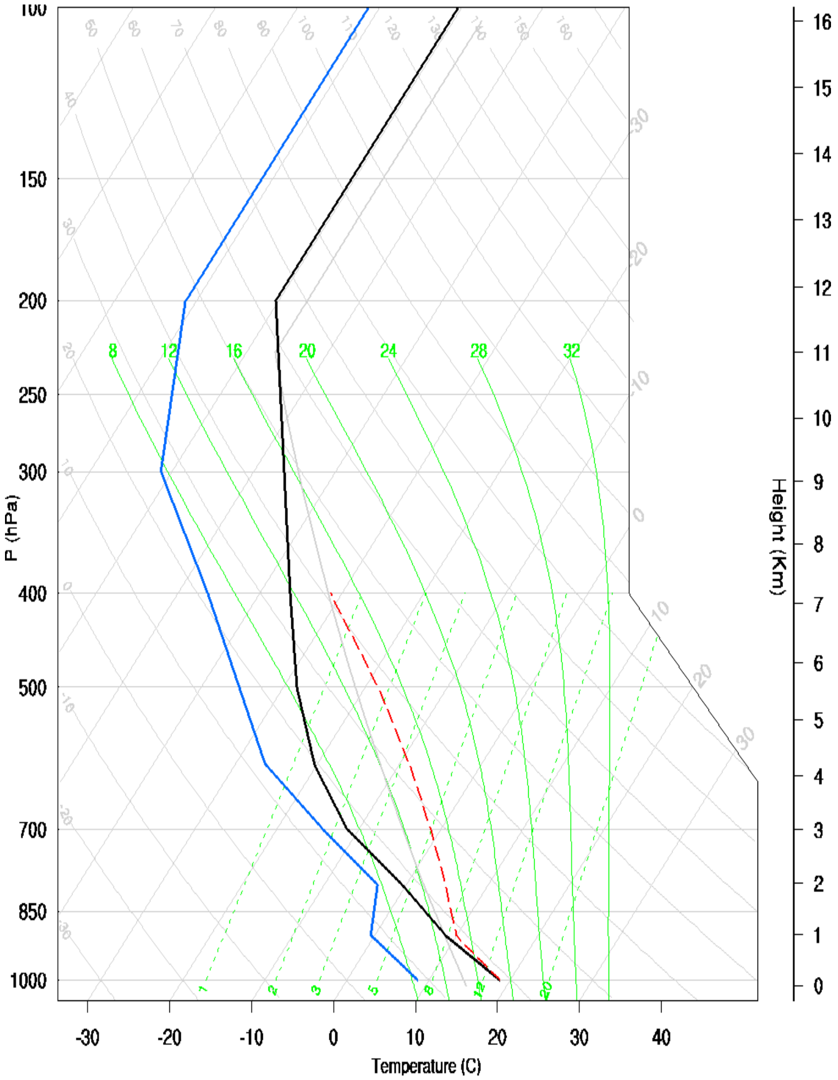
P (hPa)
100
150
200
250
300
400
500
700
850
1000
Temperature (C)
-30
-20
-10
0
10
20
30
40
Height (Km)
8
12
16
20
24
28
32

Figure 1

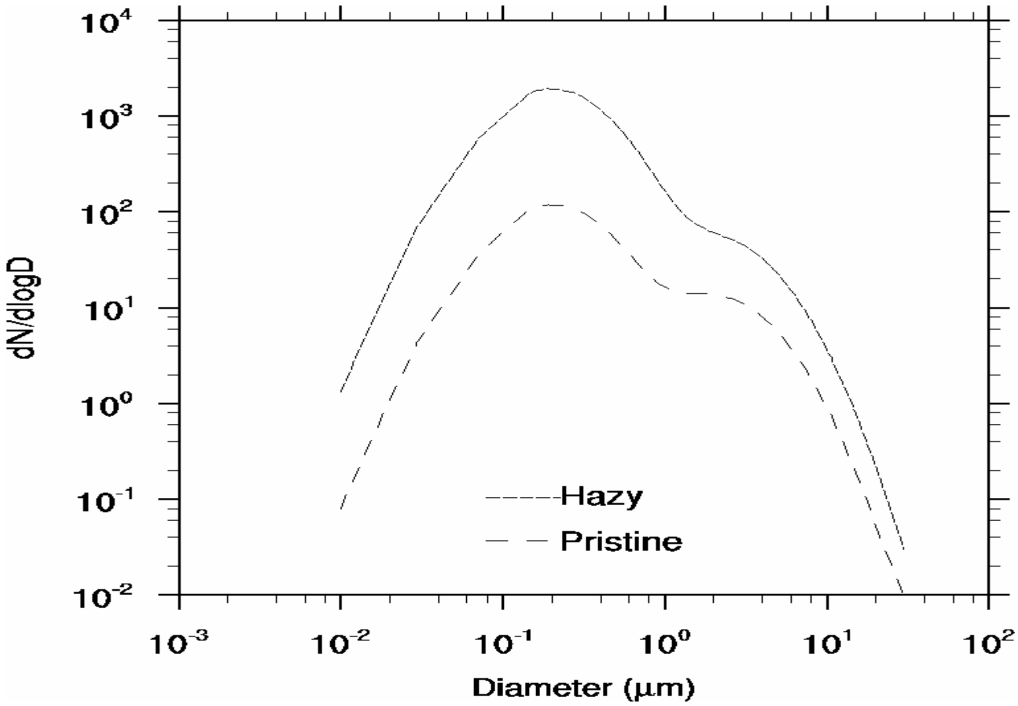

dN/dlogD
10^4
10^3
10^2
10^1
10^0
10^{-1}
10^{-2}
Hazy
Pristine
10^{-3}
10^{-2}
10^{-1}
10^0
10^1
10^2
Diameter (μm)

Figure 2

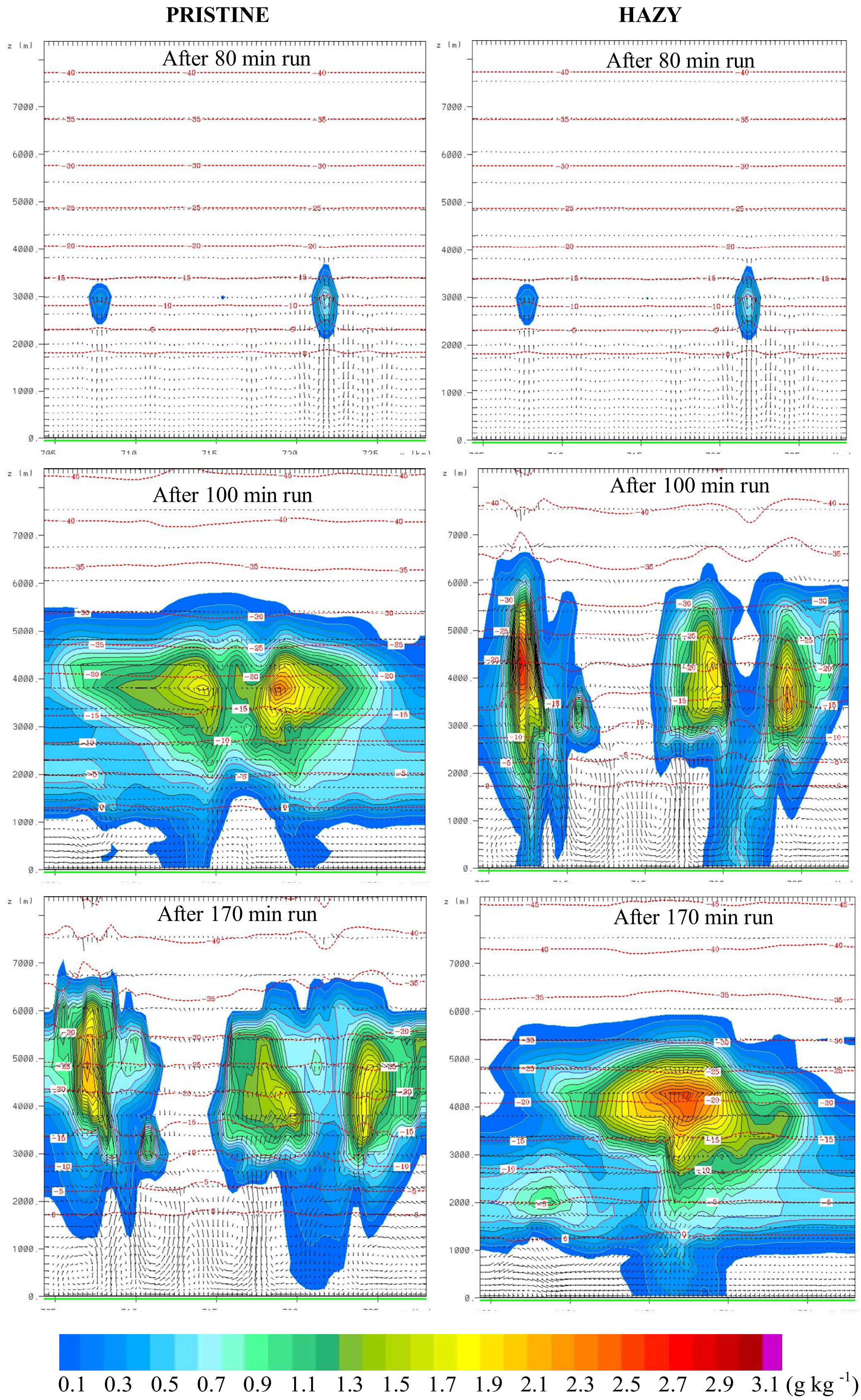
PRISTINE
HAZY
After 80 min run
After 80 min run
After 100 min run
After 100 min run
After 170 min run
After 170 min run
0.1 0.3 0.5 0.7 0.9 1.1 1.3 1.5 1.7 1.9 2.1 2.3 2.5 2.7 2.9 3.1 (g kg -1)

Figure 3

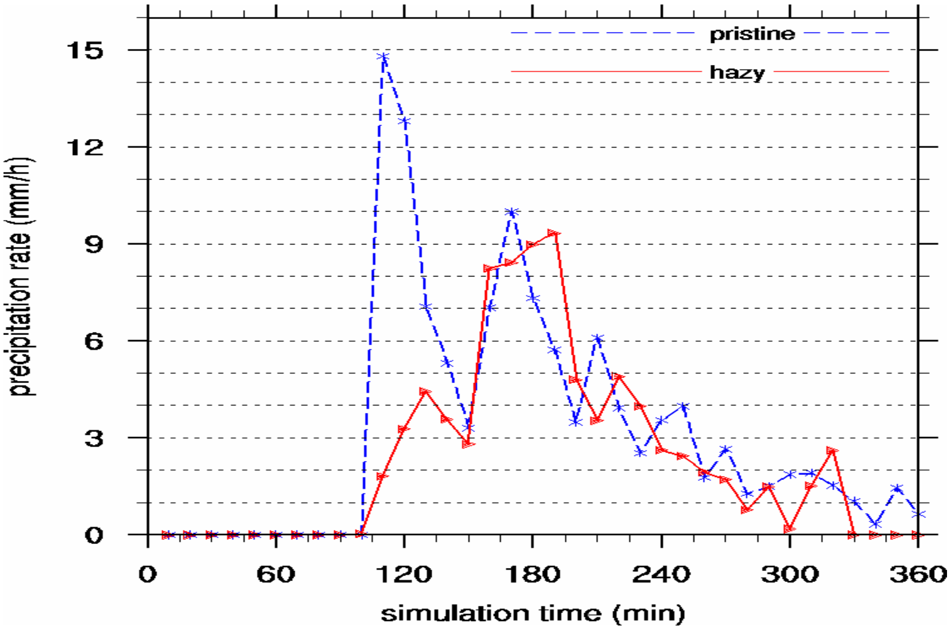
pristine
hazy
precipitation rate (mm/h)
simulation time (min)
0
3
6
9
12
15
0
60
120
180
240
300
360

Figure 4

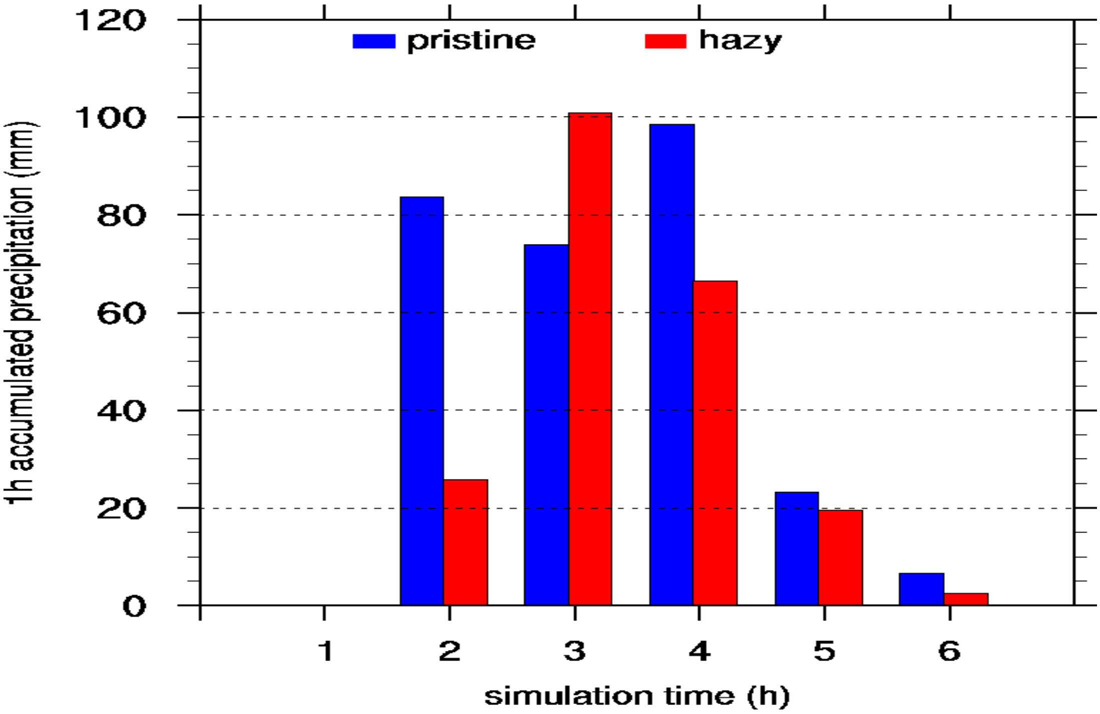
pristine
hazy
1h accumulated precipitation (mm)
120
100
80
60
40
20
0
1
2
3
4
5
6
simulation time (h)

Figure 5

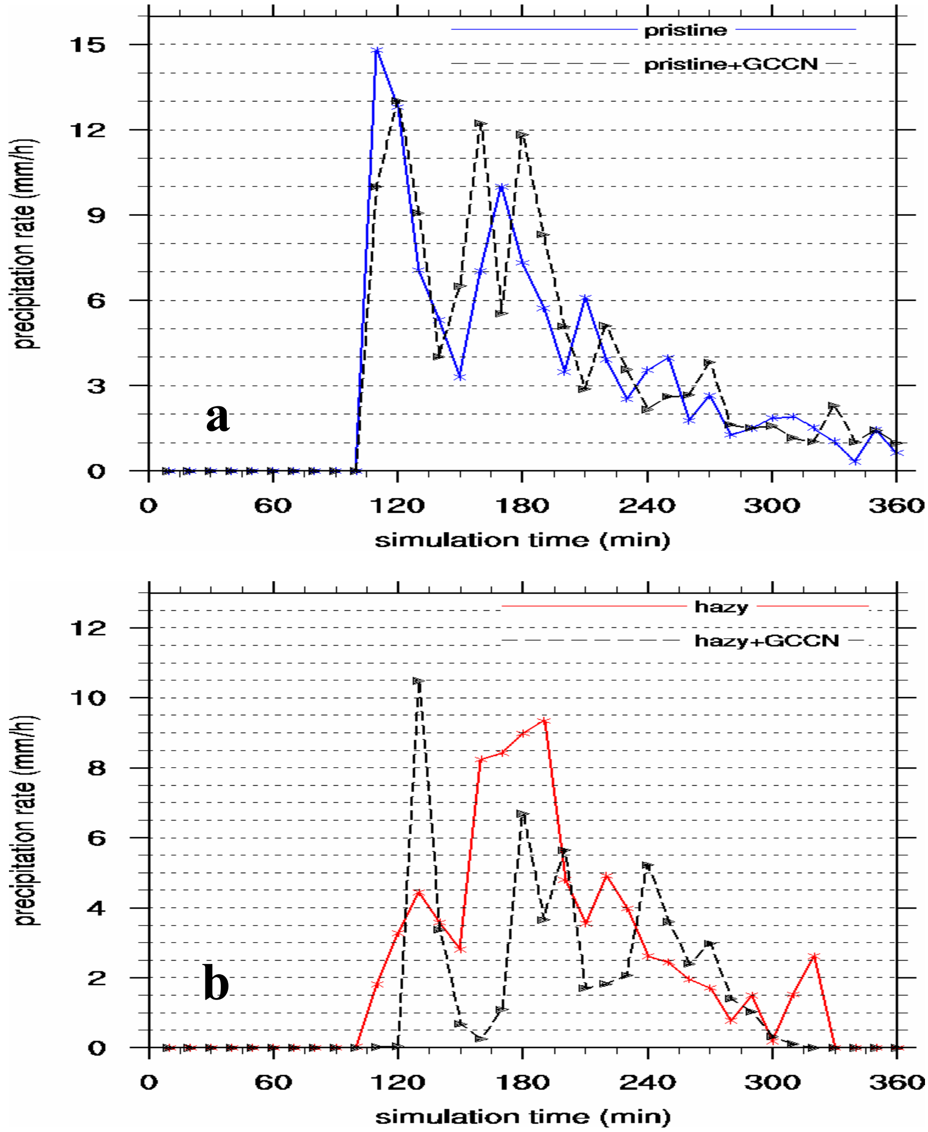

pristine
pristine+GCCN
a
precipitation rate (mm/h)
simulation time (min)
hazy
hazy+GCCN
b
precipitation rate (mm/h)
simulation time (min)

Figure 6

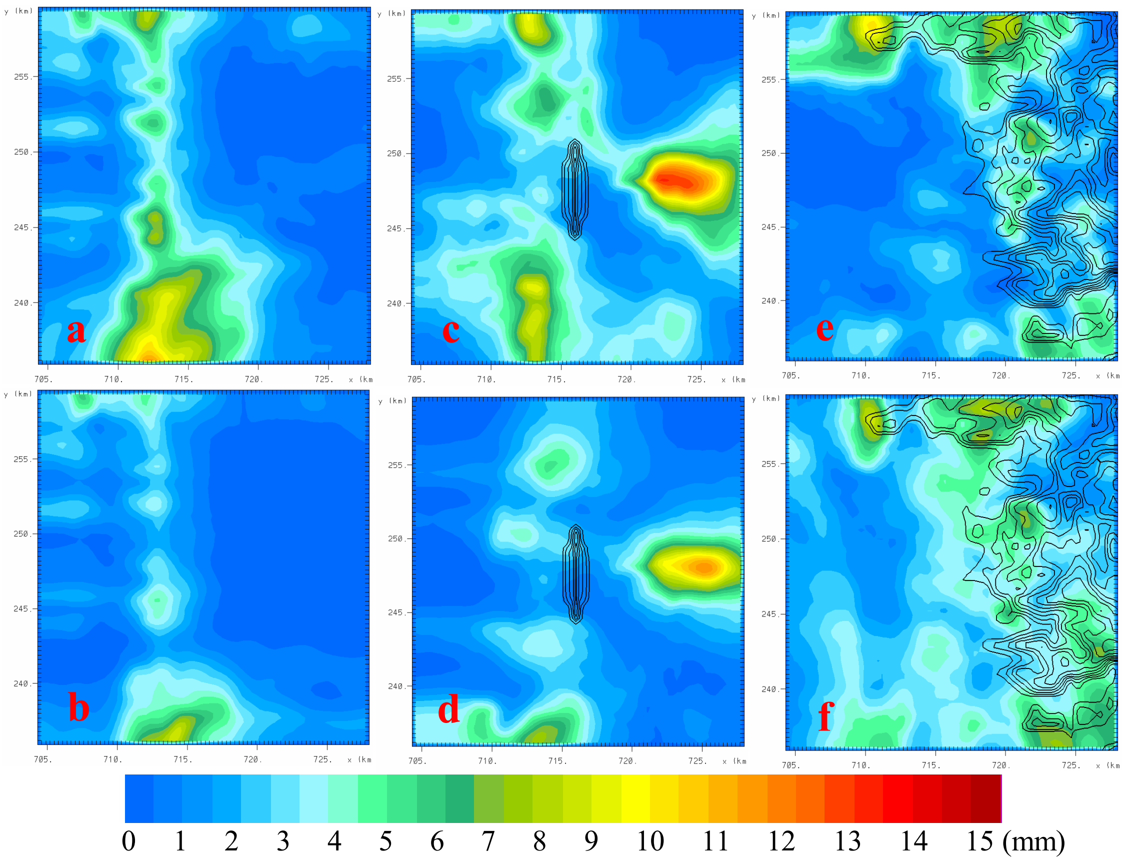

Figure 7

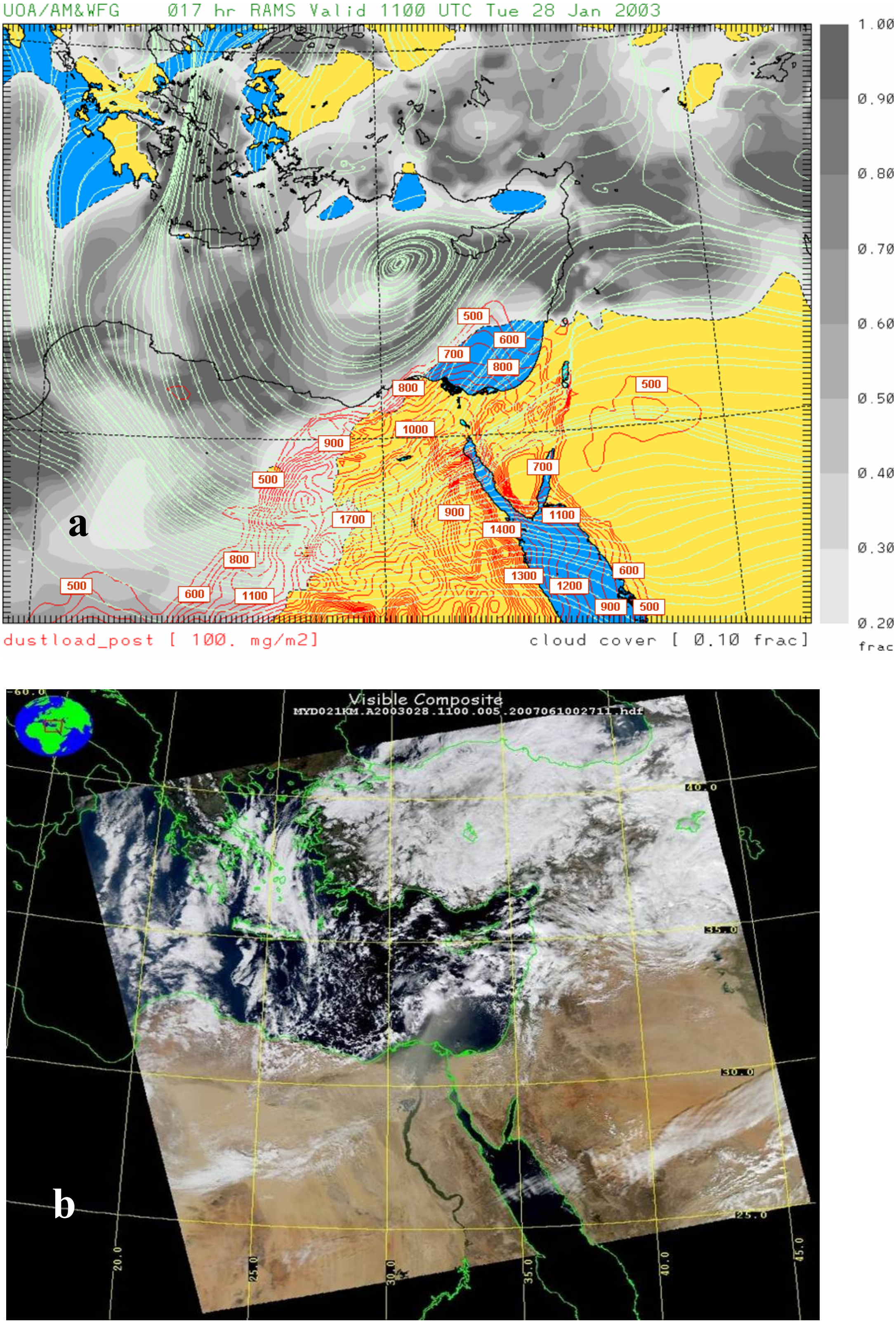
UOA/AM&WFG 017 hr RAMS Valid 1100 UTC Tue 28 Jan 2003
dustload_post [100. mg/m2]
cloud cover [0.10 frac]
1.00
0.90
0.80
0.70
0.60
0.50
0.40
0.30
0.20
frac
a
Visible Composite
MYD021KM.A2003028.1100.005.2007061002711.hdf
b

Figure 8

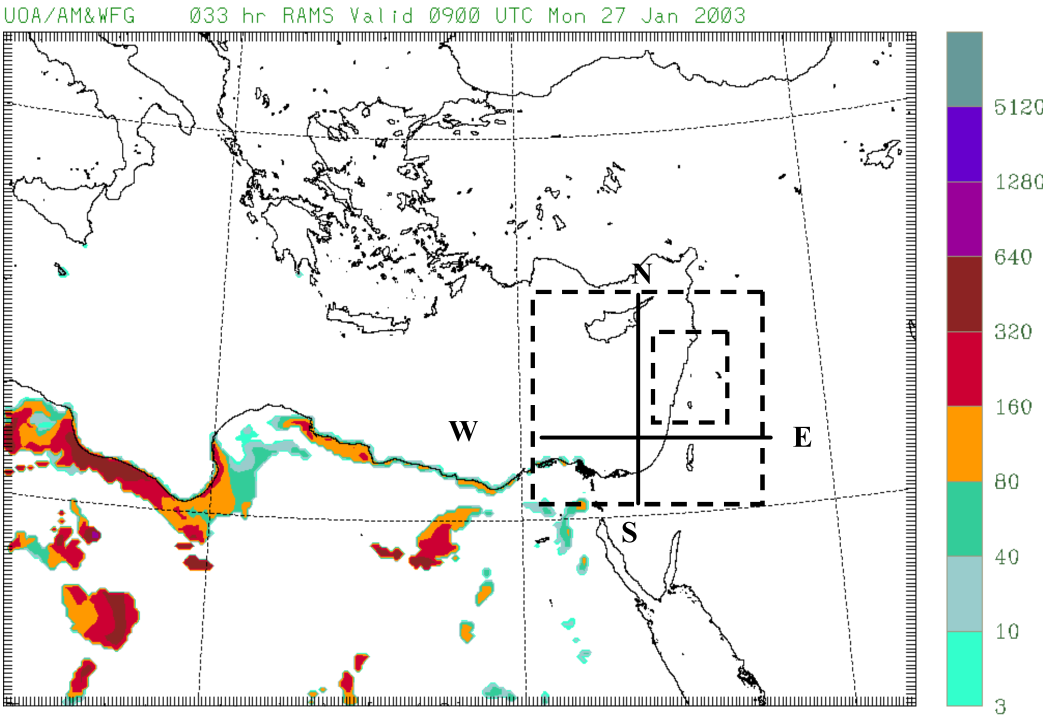

UOA/AM&WFG 033 hr RAMS Valid 0900 UTC Mon 27 Jan 2003
N
W
E
S
5120
1280
640
320
160
80
40
10
3

Figure 9

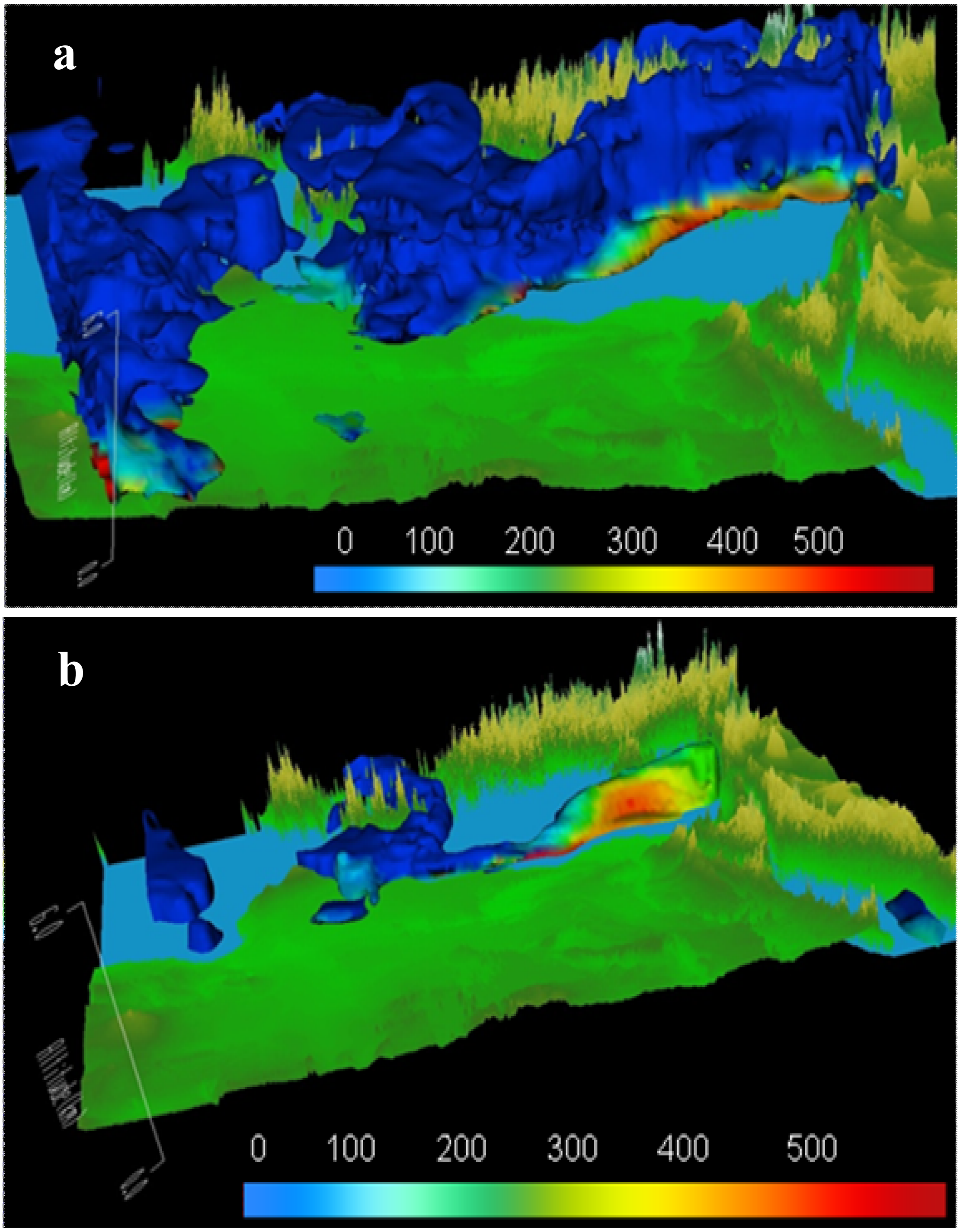

Figure 10

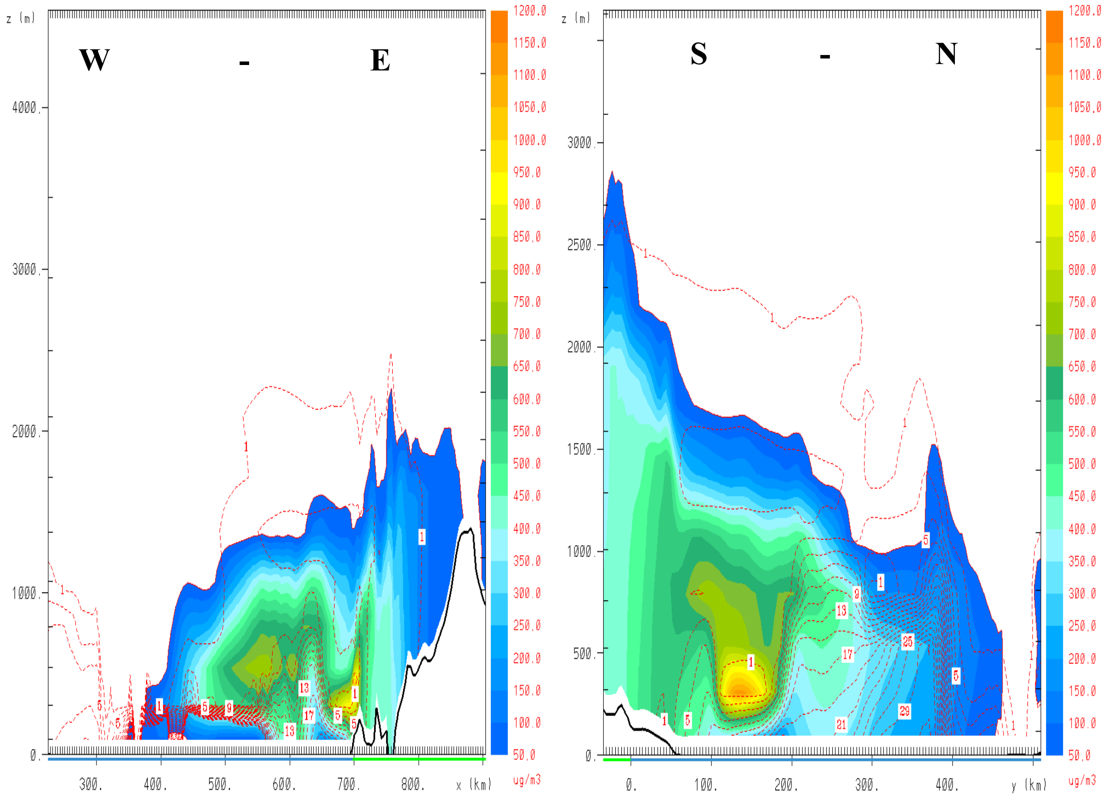

Figure 11

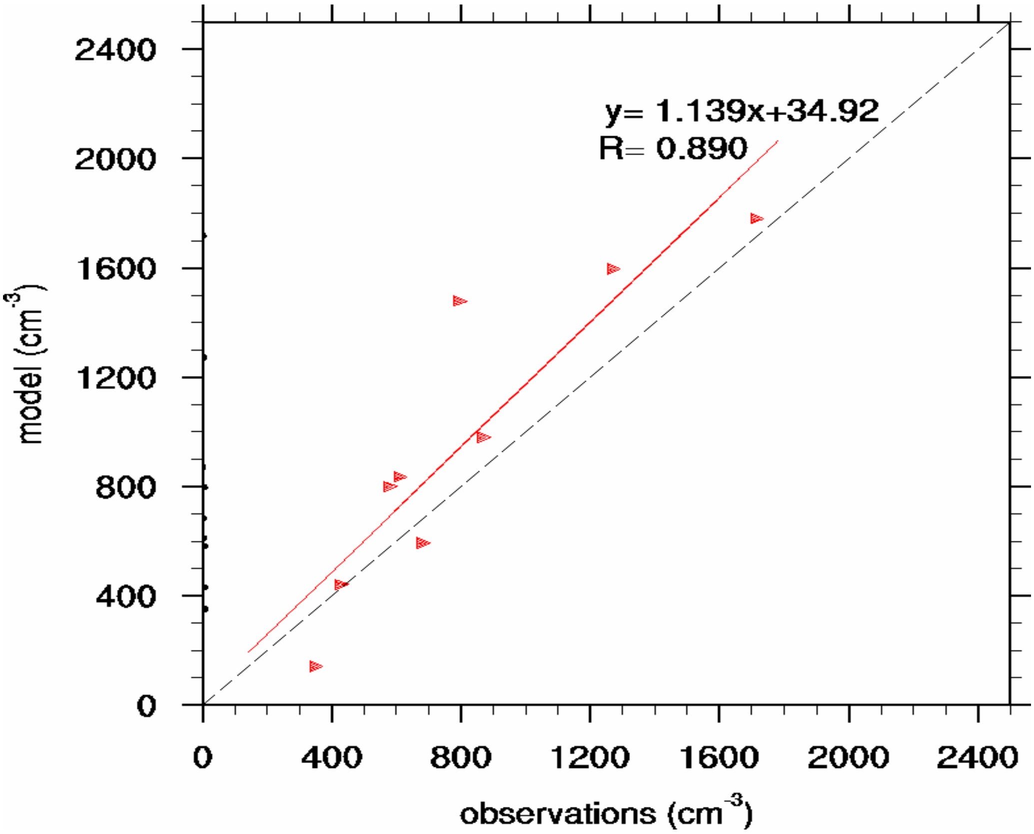

y= 1.139x+34.92
R= 0.890
model (cm-3)
observations (cm-3)
0
400
800
1200
1600
2000
2400

Figure 12

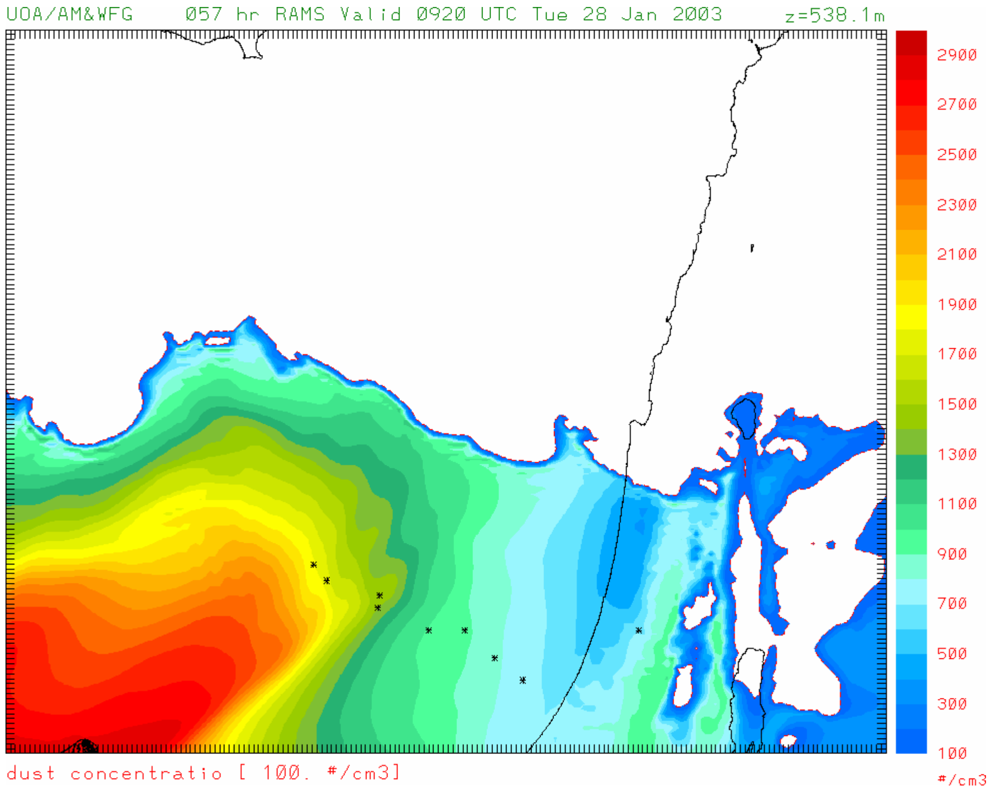
UOA/AM&WFG 057 hr RAMS Valid 0920 UTC Tue 28 Jan 2003 z=538.1m
dust concentratio [100. #/cm3]
2900
2700
2500
2300
2100
1900
1700
1500
1300
1100
900
700
500
300
100
#/cm3

Figure 13

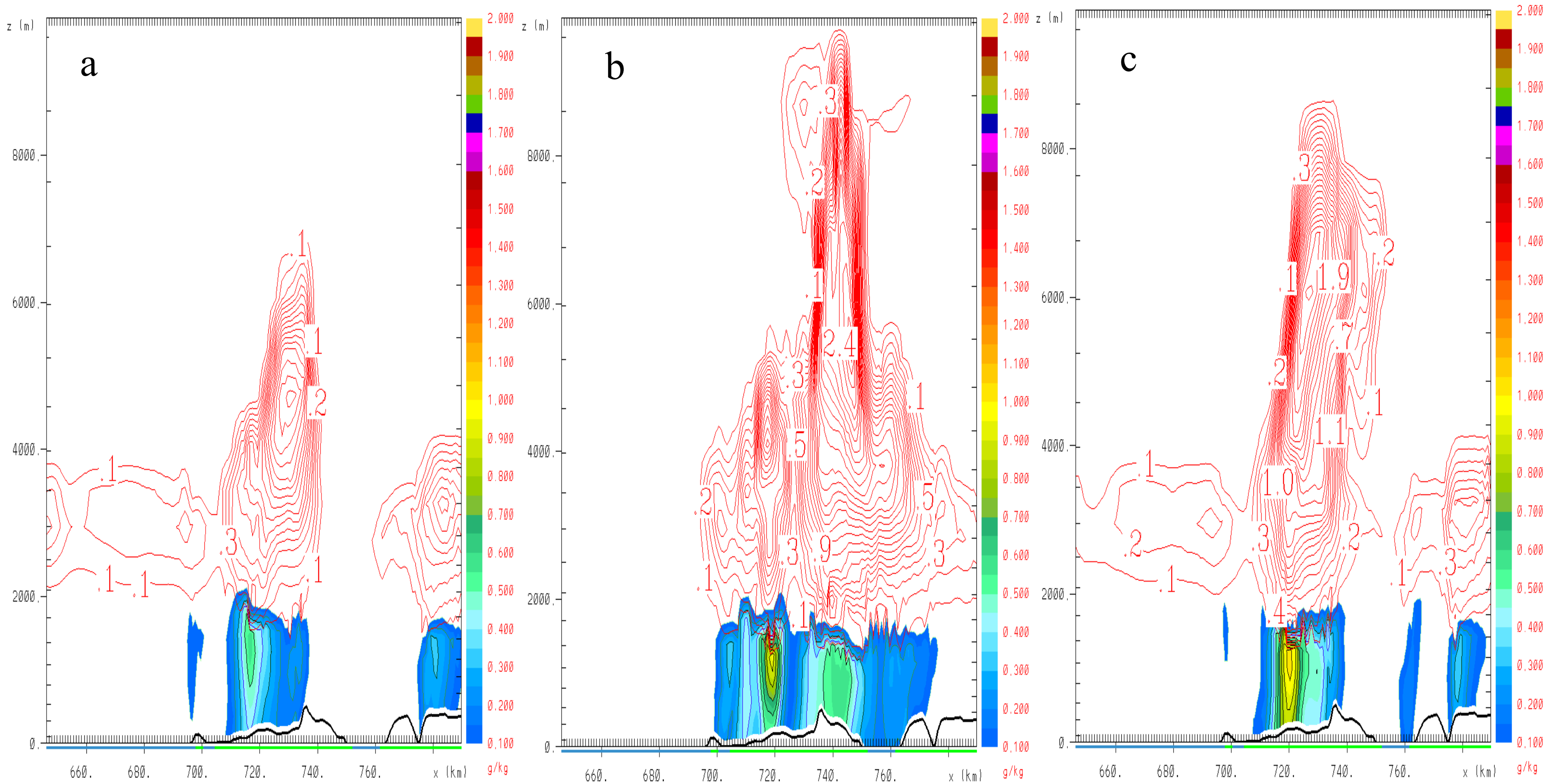

Figure 14

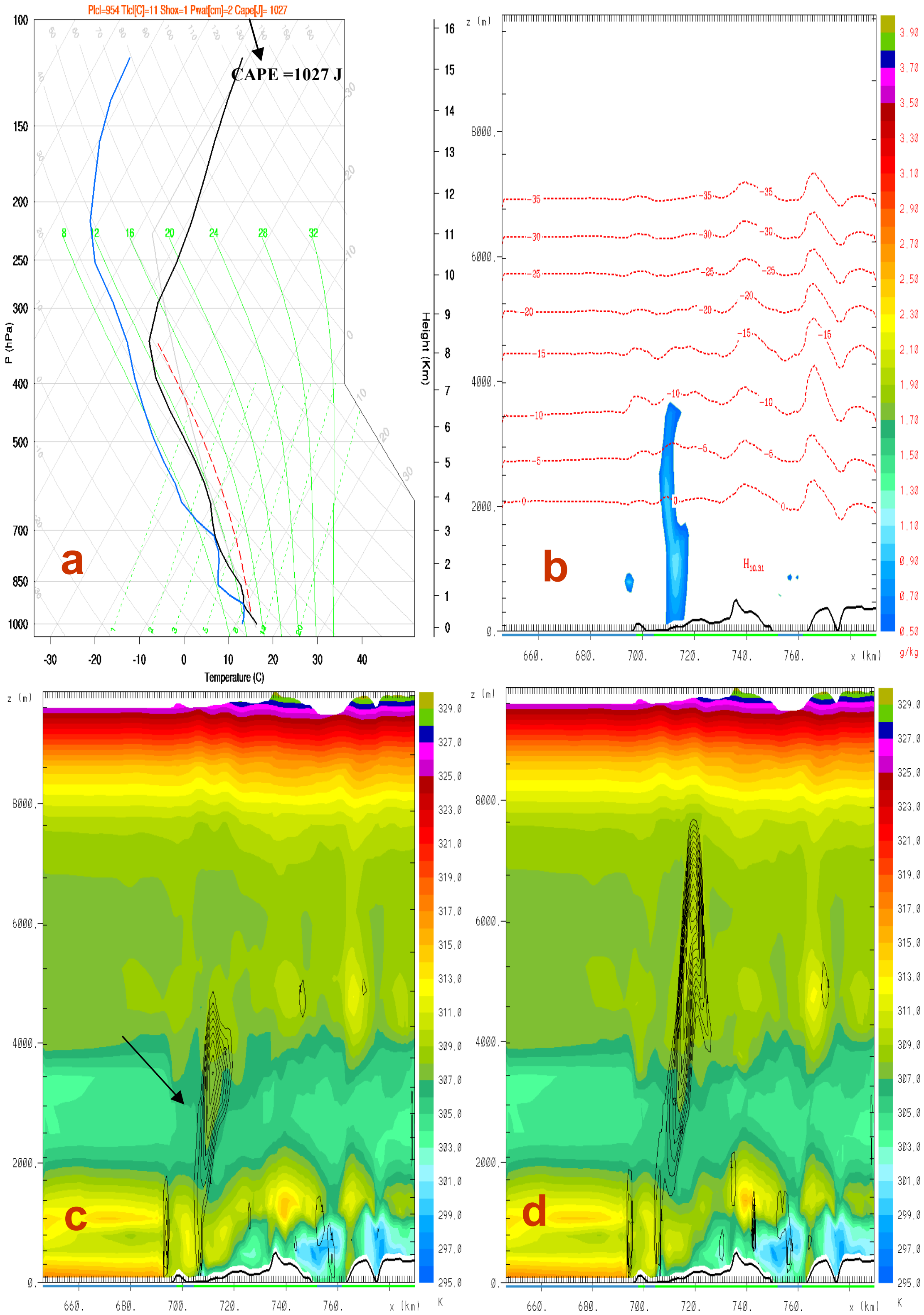
Plcl=954 Tlcl[C]=11 Shox=1 Pwat[cm]=2 Cape[J]= 1027
CAPE =1027 J
a
b
c
d
Temperature (C)
P (hPa)
Height (Km)
z (m)
x (km)
g/kg
K

Figure 15

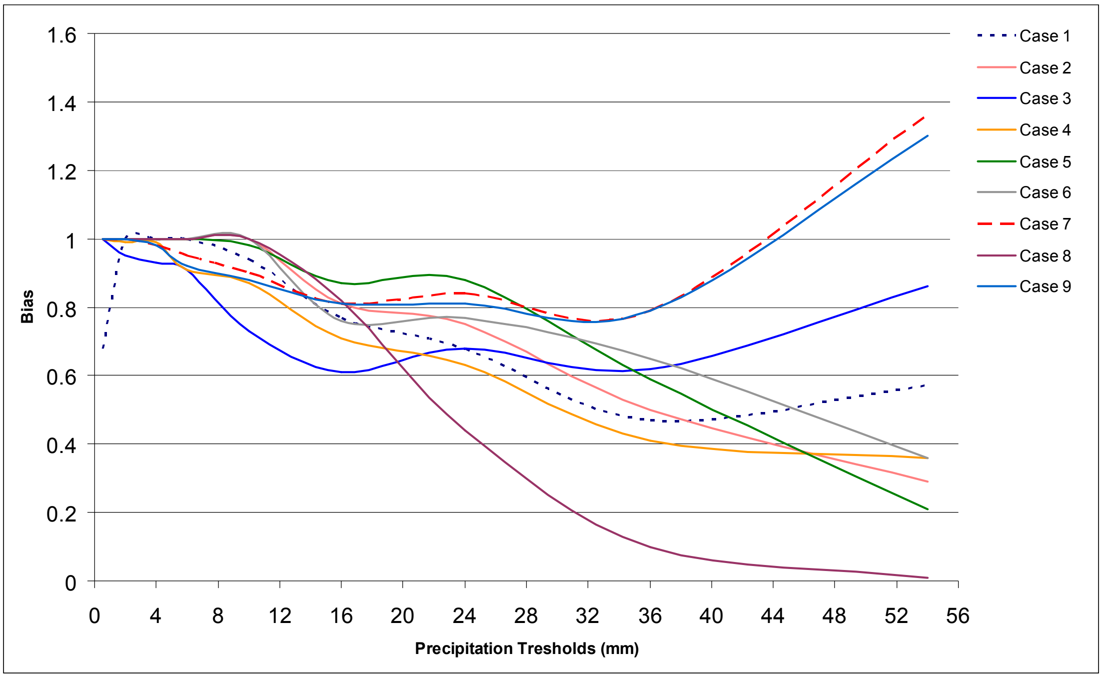
Bias
Precipitation Tresholds (mm)
1.6
1.4
1.2
1
0.8
0.6
0.4
0.2
0
0
4
8
12
16
20
24
28
32
36
40
44
48
52
56
Case 1
Case 2
Case 3
Case 4
Case 5
Case 6
Case 7
Case 8
Case 9

Figure 16

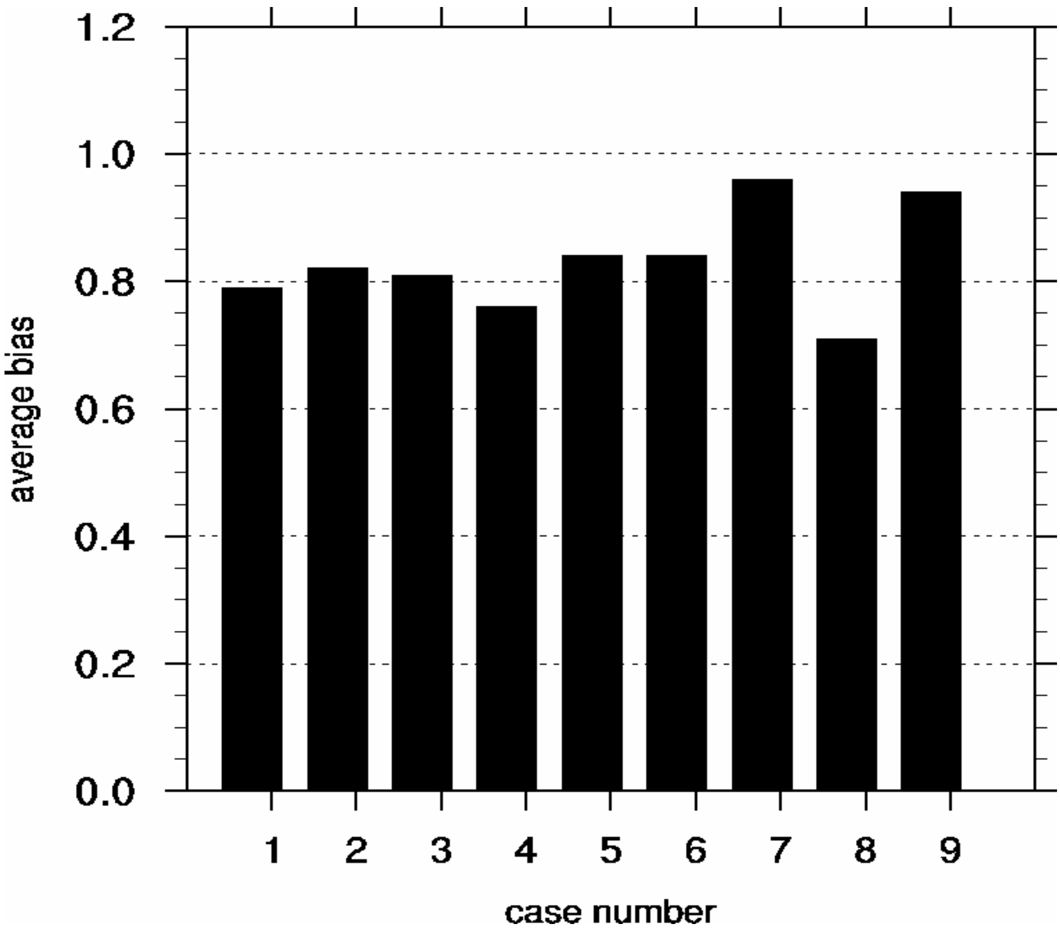

Figure 17